Discover Applied Sciences

Research

Petrogenesis and tectonic setting of the mafic rocks from the Mfengou-Manki area, Central Cameroon Shear Zone: constraints from petrology and bulk-rock geochemistry

Zakari Nchouwet[1] · Benjamin Ntieche[2] · Rose Yongue Fouateu[1] · Mama Ntoumbe[4] · Mahomed Aziz Mounjouohou[3] · Chimene Grace Staelle Atsalang[1] · Marcelle Nathalie Abomo Olomo[4] · Moundi Amidou[1]

Received: 15 August 2023 / Accepted: 27 November 2023
Published online: 29 February 2024

Abstract
In the Central Cameroon Shear Zone, several studies were focused on granitoids and very few on mafic rocks. Here we report the petrography, geochemistry and mineralogy of the Mfengou-Manki mafic rocks in order to constrain their petrogenesis and tectonic settings and the role of lithospheric and asthenospheric mantle sources in their genesis. The studied mafic rocks are subdivided into columnar jointed basalts and mafic dykes. Clinopyroxene thermobarometry indicates that the mafic dykes crystallized at a temperature of 1071 to 1193 °C and a pressure of 4 to 12 kbar while the columnar jointed basalts emplaced at a temperature of 1064 to 1152 °C and 2 to 13 kbar pressure. The mafic dykes and columnar jointed basalts present high La/Sm, Sm/Yb, Nb/Yb and Th/Yb ratios, indicating garnet to spinel transition zone mantle source. The multi-element diagram of the mafic dykes display enrichment in Nb, Ta, Pb and Ti and depletion in Th, U, Ce and Zr compared to that of the columnar jointed basalts (slight depletion in Nb and Ta and pronounced depletion in U, Pb and Zr and enrichment in Cs, Ba and Rb) indicating the little involvement of the sub-continental lithospheric mantle to the formation of the columnar jointed basalts. The Nb/La ratio > 1 for the mafic dykes and < 1 for the columnar jointed basalts also suggest the derivation of the mafic dykes from the asthenospheric mantle and the columnar jointed basalts from the mixed lithospheric-asthenospheric mantle due to the sub-continental lithospheric mantle delamination under the Central Cameroon Shear Zone.

Article Highlights

- The mafic rocks of the Mfengou-Manki area in the Central Cameroon Shear Zone are of two types, namely the mafic dykes and the columnar jointed basalts.
- The mafic dykes are calc-alkaline to tholeiitic and derived from the asthenospheric mantle, while the columnar jointed basalts are essentially calc-alkaline and from the mixed asthenospheric and lithospheric mantle. The mafic dykes emplaced at a temperature of 1071 to 1193 °C and a pressure of 4 to 12 kbar while the columnar jointed basalts emplaced at a temperature of 1064 to 1152 °C and 2 to 13 kbar pressure.
- The delamination of the sub-continental lithospheric mantle under the Central Cameroon Shear Zone in the Adamawa Yade domain and the West Cameroon domain may have favored the ascend of the plume-derived melts that could have imparted into sub-continental lithospheric mantle through the plume- lithosphere interaction.

✉ Zakari Nchouwet, nchouwetzakari10@yahoo.com | [1]Department of Earth Sciences, University of Yaounde 1, P.O. Box 812, Yaounde, Cameroon. [2]Geology Laboratory, Higher Teacher Training College, University of Yaounde 1, P.O. Box 47, Yaounde, Cameroon. [3]Department of Earth Sciences, University of Maroua, P.O. Box 814, Maroua, Cameroon. [4]School of Geology and Mining Engineering, University of Ngaoundere, P.O. Box: 115, Meiganga, Cameroon.

Keywords Mfengou-Manki · Mafic rocks · Geochemistry · Thermobarometry · Mantle

1 Introduction

The emplacement of mafic dykes in any plutonic or metamorphic basement is very important for the understanding of geological events over time as they act as an important time marker in the geological record [1]. The geochemistry of mafic dykes also provides important information for the proper understanding of the origin of magmas, their melting conditions and tectonic events in subduction zones [2, 3]. The sources of magma for mafic or intermediate dykes emplaced within the crust are multiple and include among others, the sub-continental lithospheric mantle, plume–lithosphere interaction and the contamination of mantle magma by the crust [4–7]. Moreover, it is also demonstrated that fluids and magma generated from subducted plates and subducted sediments can also participate in the generation of mafic dykes' magma in a convergent zone [8]. Several geodynamic processes have been shown to explain the formation of dykes. These include: (1) lithospheric distension or plate opening [9–12]; (2) subduction of oceanic plate [13, 14]; (3) arc collision [15, 16]; and (4) continental collision [17].

Unlike the volcanic edifices of the Cameroon Volcanic Line (CVL), the Central Cameroon Shear Zone (CCSZ) consisting mainly of granites, gneisses and mylonites hosts very few mafic rocks. Despite this rarity, some mafic dykes have been discovered in the Magba [18] and Njimom [19] areas in the CCSZ and their origin and tectonic setting have been discussed. However, in the Mfengou-Manki area, columnar jointed basalts were not observed. Apart from the work of Kouamo Keutchafo et al. [19] who studied only the mafic dykes situated along the Foumban-Njimom highway, no author has ever studied the columnar jointed basalts of the Mfengou area because it was situated far from the main highway and hidden by a relative soil cover and vegetation. The outcrop was discovered in 2016 and was used as quarry for the Foumban-Manki road construction. Moreover, the petrology, and the extension of the mafic dykes from the Mfengou-Manki were not yet well known. This work aims firstly to study the petrogenesis and tectonic setting of the mafic dykes and the columnar jointed basalts, and secondly to study their probable rock source using the ICP AES, ICPMS and electron microprobe analytical methods.

2 Geological context

The geology of Cameroon is dominated by two main geological groups, namely the Central African Fold Belt in Cameroon (CAFB) and the Congo Craton (CC). The CAFB in Cameroon hosts the current study area and is subdivided into three domains namely, the Northwest Cameroon Domain (NWCD), the Yaounde Domain (YD), and the Adamawa Yade Domain (AYD) (Fig. 1). Located in the south of Cameroon, the Yaounde Domain is bounded in the south by the Congo Craton and in its northern sector by the Sanaga Fault (SF). The geological formations found in this area are pre- to syn-tectonic intrusive granitoids and mafic dykes with alkaline and transitional affinities and metasediments [20]. Its southern side is marked by the predominance of mafic dykes and/or serpentinized ultramafic rocks, gabbros and diorites [21]. The Adamawa Yade domain lies between the Sanaga Fault in the south and the Tchollire-Banyo Fault (TBF) in the north (Fig. 1). It is the domain that hosts the study area and consists of large Pan-African intrusions and metamorphosed Palaeoproterozoic relics emplaced during the Pan-African tectonic evolution. The Northwest Cameroon Domain (NWCD) also known as the Poli Group [22, 23] is located in the North Cameroon. It is limited in the south by the Tchollire-Banyo Fault and consists of Meso to Neo-Proterozoic volcano-sedimentary basins variably metamorphosed into gneisses and schists [24]. In places, it is covered by pre to syn- or late-tectonic intrusive calc-alkaline formations (granites, granodiorites and diorites) and metamorphosed volcanic and detrital deposits [23–25].

Located in the southern part of the Adamawa Yade domain (Central domain) (Fig. 1), precisely within the Central Cameroon Shear Zone (CCSZ), the Foumban-Magba area (hosting the study zone) is made up of granitoids subdivided into granites, gneisses, mylonites and migmatites and few mafic to intermediate rocks [18, 26–29]. The Central Cameroon Shear Zone is a Pan-African mega structure made up of lineaments oriented N70E and extending from Sudan into north-eastern Brazil [29]. This fault network allowed the upwelling of the mafic rocks magma following the C_2 shear axes and their emplacement within the granite and gneiss substratum [18]. The mafic rocks are high-K calc-alkaline to shoshonitic and are situated in the Magba area within the Foumban-Magba Zone. They are also found in the Kekem and Nyos area at the south of the CCSZ. In Magba and Kekem, they were emplaced in a subduction environment and were formed from the sub-continental lithospheric mantle with the participation of a crustal component [18]. The Mfengou-Manki area

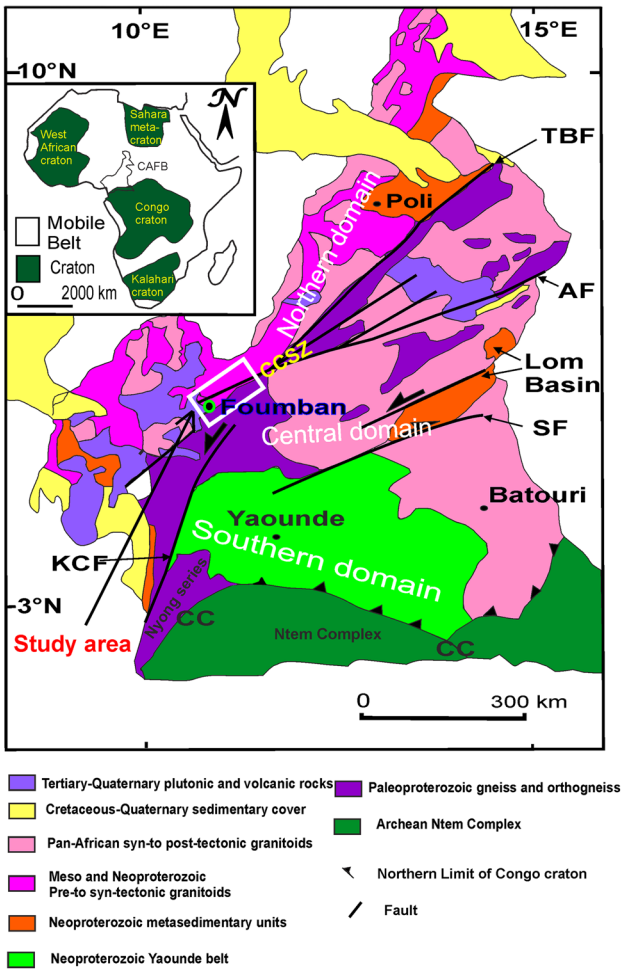

Fig. 1 Geological map of Cameroon modified after Toteu et al. [83] and Ntieche et al. [27]. The Central African Shear Zone is defined by a system of NE-trending faults comprising Tchollire-Banyo Fault (TBF), Adamawa Fault (AF), Sanaga Fault (SF), and Kribi-Campo Fault (KCF). The inset is the map of the African continent, showing the location of Cameroon relative to the distribution of cratons and mobile belts

consists of granites, migmatites, gneisses and mylonites which locally host mafic to intermediate rocks not yet studied in detail (Fig. 2).

3 Analytical methods

Representative fresh rock samples were collected during fieldwork for petrography, geochemistry and mineral chemistry studies. From the fresh samples collected in the field, thirty (30) thin sections were made. Twenty-four (24) samples (17 columnar jointed basalts, 07 mafic dykes), were selected for the whole rock geochemistry at the commercial BVM, ACME Lab, Vancouver (Canada) using inductively coupled plasma-atomic emission (ICP-AES) for major elements and inductively coupled plasma-mass spectrometry (ICP-MS) for trace elements and REE. A mixture of 0.2 g of each sample and 0.9 g of lithium metaborate/lithium tetraborate flux was prepared and melted in an oven at 1000 °C. The resulting melt was cooled and dissolved in 100 ml of 4% nitric acid and 2% hydrochloric acid. After dissolution, the solution was then analyzed by ICP-MS and the results were corrected for inter-element spectral interferences. For the Loss On Ignition (LOI) process, 1.0 g of each sample powder is placed in an oven at 1000 °C for 1 h, then cooled and weighed. The LOI (in percentage) is then calculated from the difference in weight. Different standards were used for data quality assurance.

For mineral chemistry, four samples (02 mafic columnar joints and 02 mafic dykes) were selected. The observed mineral assemblages were imaged, and mineral compositions were measured using a CAMECA SX 100 (15 kV, 10 nA) electron microprobe at the Pierre et Marie Curie University, Paris VI, France. Standards used were diopside for Mg, Ca and Si, Fe_2O_3 for Fe, $MnTiO_3$ for Ti and Mn, Cr_2O_3 for Cr, albite for Na, and orthoclase for K and Al. Counting times were 10 s for both peaks and background, with a 5 µm defocused beam.

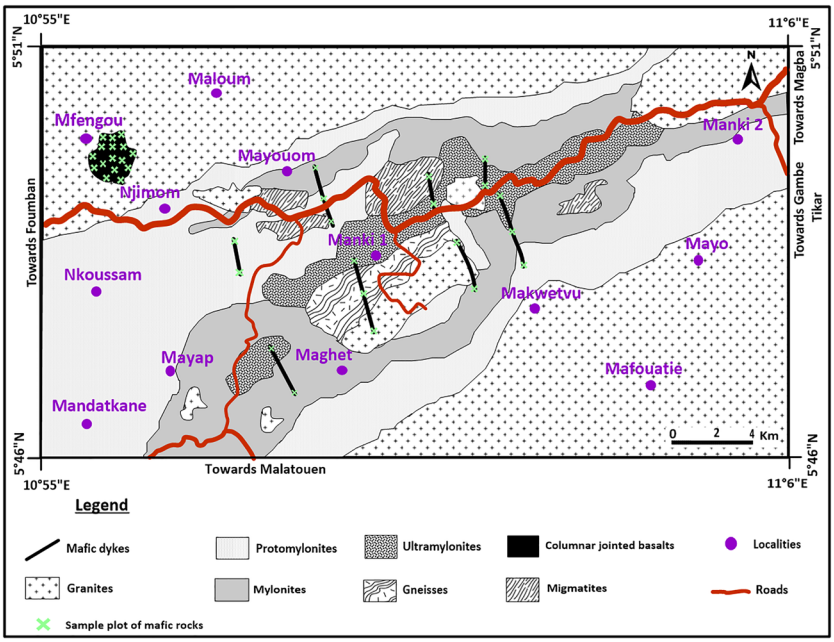

Fig. 2 Geological sketch map of the study area

4 Results

4.1 Field relationship

Columnar jointed basalts are located in the NW of the study area, at about 4 km from the main road joining Foumban to Magba (Fig. 2). They occur at the hilltop within the granite substratum and are oriented E-W to NE-SW. The outcrop appears as a crater (about 800 m long over 500 m wide). The columns are vertical, inclined, or horizontal and display mostly sections showing pentagonal and hexagonal shape with a side measuring about 20 to 50 cm (Fig. 3a, b). Some columns faces display erosion crust with orange to yellowish color due to alteration. The rock is melanocratic and display aphyric to microlitic texture.

Mafic dykes are exposed only on the shear band belonging to the Foumban-Bankim Shear Zone. The shear band measures about 10 km in width and 18 km long. The dykes are melanocratic displaying fine to medium-grained texture and crosscut the granites, mylonites and gneisses. They are exposed in the Chinsap, Chinpouet, Mayouom, Mayap and Vuh-Ngouo areas. At the Vuh-Ngouo hill and Mayap area, the mafic dykes crosscut the gneisses and mylonite, while at the Chinsap, Mayouom and Chinpouot, they crosscut the mylonite and granite.

All the dykes strike NW–SE to NNW-SSE. The dykes' outcrops present variable sizes varying from 20 cm to 3 m width and from 10 to 20 m length (Fig. 3c, d). They present mostly a sharp contact with their host rock.

4.2 Petrography

4.2.1 Columnar jointed basalts

Columnar jointed basalts have microlitic textures and consist mainly of plagioclase (20–40 vol.%), pyroxene (20–30 vol.%), chlorite (5–15 vol.%), olivine (5–10 vol.%), opaques (1–15 vol.%), K-feldspar (2–7 vol.%) and calcite (1–3 vol.%) (Fig. 4a). Plagioclases occur as elongated microslats together with K-fedspar in the groundmass surrounding olivine and pyroxene phenocrysts. In some sections prepared from the inclined columnar, the plagioclase crystals are well aligned, indicating the magma flow direction (Fig. 4a). Pyroxenes form isolated globular or elongated phenocrysts and microcrysts in the groundmass. Some crystals are altered into iddingsite or chlorite. In places, numerous pyroxene microcryts form a rim around quartz xenocrysts testifying to the fact that the quartz crystals were taken from the host granite-gneissic substratum by the mafic magma during its ascent to the surface (Fig. 4b). Olivines are less abundant in the rock and present globular shape. They are in place altered into serpentine (Fig. 4a). Calcite occurs as subhedral phenocrysts and displays its characteristic twining although attacked at its edges by some alteration reaction (Fig. 4b).

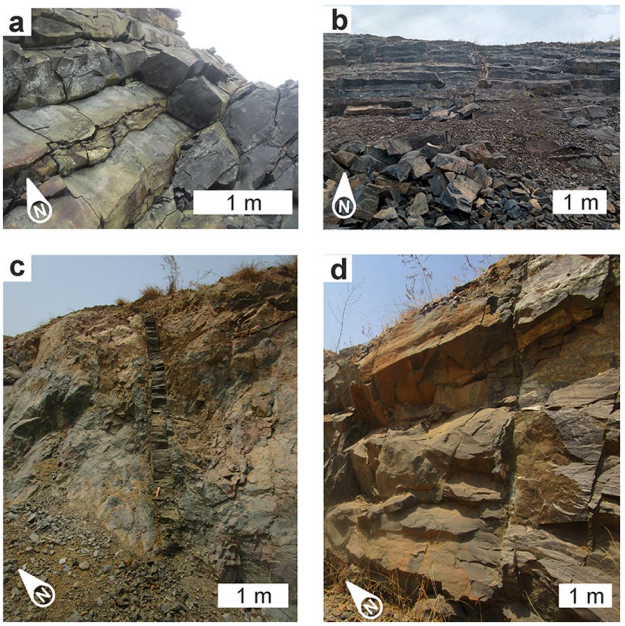

Fig. 3 Field photographs of the studied mafic rocks. **a** Inclined columnar jointed basalts at Mfengou, **b** Horizontal columnar jointed basalts, **c** Mafic dyke crosscutting ultramylonite host rock at Nchinsap village, **d** Mafic dyke occurring in the Vuh-Ngouo cliff. Note the thickness of the dyke and its sharp contact with the host mylonite

4.2.2 Mafic dykes

Mafic dykes are fine to medium-grained (Fig. 4c, d). They consist of plagioclase (20–40 vol.%), pyroxene (15–35 vol.%), olivine (5–10 vol.%), opaque (5–8 vol.%), K-feldspar (2–8 vol.%) and chlorite (1–5 vol.%) (Fig. 4c, d). K-feldspars are mainly sanidine and are in place crosscutting plagioclases laths. In places, they show their characteristic clear appearance and simple twining. Plagioclases occur as elongated laths radially oriented while pyroxene appears only as microcrystals in the groundmass. Olivines are in the form of subhedral and anhedral crystals locally associated with pyroxenes and plagioclases. Some crystals show serpentinization reaction (Fig. 4d).

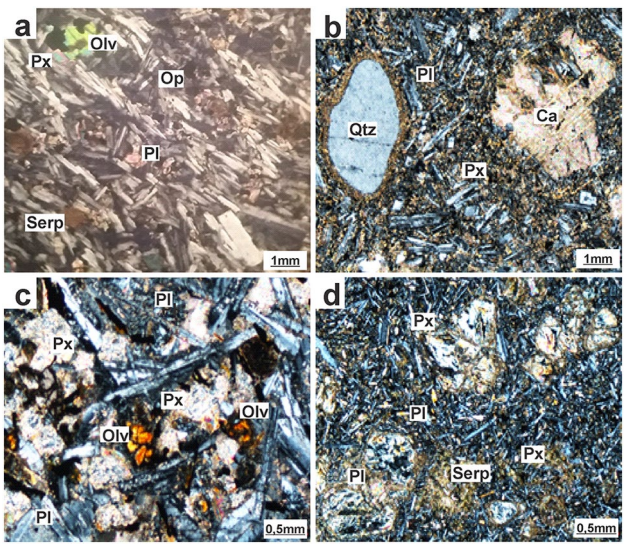

Fig. 4 Photomicrographs of mafic rocks' thin sections. **a** Columnar jointed basalts displaying a microlitic texture. Note the orientation of the plagioclase laths indicating the magma flow direction, **b** Columnar jointed basalts presenting quartz xenocryst surrounded by pyroxene microcrystals forming a reaction rim testifying that the quartz crystal was ripped from the ganito-gneissic substratum by the mafic magma during its ascent to the surface, **c** Medium-grained texture in mafic dykes, **d** Plagioclase laths surrounding relics of olivine crystals that underwent the serpentinization process

4.3 Mineral chemistry

4.3.1 Feldspars

Feldspar analyses are shown in Table 1. In mafic dykes, K-feldspars are orthoclase, sodic sanidine and potassic albite with orthoclase content ranging from Or_{11} to Or_{85} (Fig. 5a). Plagioclases display a wide composition range, varying from potassic oligoclase to potassic labradorite (An_{32-55}) (Fig. 5a). The columnar jointed basalts show a wide K-feldspar composition ranging from sanidine to calcio-potassic albite (Or_{06} to Or_{64}) and the plagioclase ranging from labradorite to oligoclase (An_{23} to An_{58}). The feldspar present very high FeO content (18.24- 30.07 wt%) and low Al_2O_3 (0.13–0.58 wt%) and MgO (0.03–0.31 wt%) testifying to the substitution of Al^{3+} and Mg^{2+} by the Fe^{3+} [30].The mafic dyke's feldspars globally present similar chemical characteristic as the Njimom dykes [19] (within this study area), but the chemistry of the feldspar of the mafic columnar is different from that of the mafic dykes and the Njimom dykes (Fig. 5a).

4.3.2 Pyroxene

Representative microprobe analyses of the pyroxenes and their calculated structural formulae based on six oxygen end-members are presented in Table 2. Pyroxenes are essentially clinopyroxenes and show a restricted compositional range, with Al_2O_3 (2.33–4.86), FeO_t (10.01–17.98), MgO (8.02–13.08), CaO (19.81–21.98) and TiO_2 (0.08–2.45) concentrations in mafic dykes and Al_2O_3 (3.98–6.52), FeOt (10.22–12.18), MgO (11.45–12.97), CaO (19.89–21.86) and TiO_2 (0.97–3.65) content in columnar jointed basalts (Table 2). The studied pyroxenes' mineral composition falls within Wo_{43-50}, En_{25-39} and Fs_{15-24} for the mafic dykes and Wo_{43-49}, En_{36-42} and Fs_{09-17} for the columnar jointed basalts. On the Wo-En-Fs ternary diagram after Morimoto et al. [31], most of the samples fall within the augite field and few in the diopside field (Fig. 5b). The chemistry of pyroxenes of the mafic dykes and mafic columnar joints are similar to those of the Njimom dykes [19] (Fig. 5b).

4.4 Thermobarometry and oxygen fugacity of the magma

Temperature and pressure of the crystallization of numerous minerals are generally used to understand the emplacement conditions of igneous or metamorphic rocks. Several thermo-barometers were used to estimate the pressure and temperature of the crystallization of the mafic dykes and columnar jointed basalts from the Mfengou-Manki area, but three of them have been retained for this work because they don't compulsorily need the simultaneous presence of two pyroxenes (orthopyroxene and clinopyroxene) and can also be used for both Mg-Ca-Fe and Fe–Mg pyroxenes. The first one is the method used by Soesoo [32] for the formation temperature of pyroxenes. In that method, XPT and YPT indices (Fig. 6a) are used, and are based on the following equations:

a) $XPT = 0.446\ SiO_2 + 0.187\ TiO_2 - 0.404\ Al_2O_3 + 0.346\ FeO - 0.052\ MnO + 0.309\ MgO + 0.446\ CaO - 0.446\ Na_2O$.
b) $YPT = -0.369\ SiO_2 + 0.535\ TiO_2 - 0.317\ Al_2O_3 + 0/232\ FeO + 0/235\ MnO - 0.516\ MgO - 0/167\ CaO - 0/153\ Na_2O$, where XPT and YPT are respectively the scores of the first and second eigen- vectors [32].

This method allows distinction of clinopyroxenes crystallizing from basaltic magmas over a large range of temperature (1100–1300 °C) and pressure (0–20 kbar) [32].

According to that method, the crystallization temperature of clinopyroxenes from the studied rocks ranges from 1100 to 1150 °C for the mafic dykes and from 1150 to 1200 °C for the columnar jointed basalts under the respective pressure of crystallization varying from 2 to 6 Kbar for the mafic dykes and from 6 to 15 kbar for the columnar jointed basalts (Fig. 6a, b).

Using the thermobarometric calculation after Nimis and Taylor [33] on clinopyroxenes at 3 kbar, the temperature of crystallization of clinopyroxenes ranges from 1091 to 1233 °C for the mafic dykes and from 1120 to 1229 °C for the columnar jointed basalts. When plotted on the clinopyroxene barometry diagram after Helz [34], all samples plot within the low to medium-pressure igneous rock fields (Fig. 6c). Putirka [35] established the thermometers and barometers specific for volcanic systems. This thermobarometer is most suitable for this work because the rocks are volcanic (columnar jointed basalts) and hypabyssal (mafic dykes) in origin. The temperature and pressure calculations using those thermometers and barometers give a wide range of temperature of clinopyroxene crystallization varying from 1064 to 1152 °C for the columnar jointed basalts and from 1071 to 1193 °C for the mafic dykes under

Table 1 Representative chemical composition (wt%) and structural formulae of feldspar from the Mfengou-Manki mafic rocks

Rock type		Mafic dykes									
Major oxides (%)											
SiO_2	63.14	57.66	57.01	59.39	61.76	65.14	60.45	57.01	59.39	55.98	54.51
TiO_2	0.07	0.06	0.01	0.07	0	0	0.01	0.01	0.07	0.11	0.05
Al_2O_3	0.39	0.49	0.22	0.45	0.55	0.51	0.58	0.22	0.45	0.16	0.3
FeO	18.24	26.5	24.29	24.5	23.84	19.02	23.71	24.29	24.5	26.15	27.13
MnO	0.02	0	0.04	0	0	0.07	0	0.04	0	0	0.02
MgO	0.03	0.04	0.03	0.12	0.12	0.31	0.2	0.03	0.12	0.07	0.05
CaO	0.44	1.3	7.39	1.53	1.23	0.49	3.01	7.39	1.53	9.13	10.31
Na_2O	2.41	7.55	8.08	8.07	9.09	12.9	9.3	8.08	8.07	7.62	7
K_2O	15.71	5.7	1.93	4.51	3.56	1.78	3.18	1.93	4.51	1.17	0.94
Total	100.45	99.35	99.02	98.68	100.15	100.3	100.47	99.02	98.68	100.42	100.35
Calculated mineral formulae* (apfu)											
Si	2.514	2.322	2.303	2.407	2.467	2.598	2.407	2.303	2.407	2.230	2.173
Ti	0.021	0.027	0.012	0.024	0.029	0.027	0.031	0.012	0.024	0.009	0.016
Al	0.003	0.002	0.001	0.003	0.000	0.000	0.000	0.001	0.003	0.005	0.002
Fe	1.453	2.134	1.962	1.986	1.904	1.517	1.888	1.962	1.986	2.083	2.163
Mn	0.001	0.000	0.004	0.000	0.000	0.006	0.000	0.004	0.000	0.000	0.002
Mg	0.002	0.003	0.002	0.010	0.010	0.025	0.016	0.002	0.010	0.006	0.004
Ca	0.035	0.105	0.597	0.124	0.098	0.040	0.239	0.597	0.124	0.728	0.822
Na	0.384	1.216	1.305	1.309	1.453	2.065	1.482	1.305	1.309	1.215	1.117
K	2.502	0.918	0.311	0.732	0.569	0.284	0.508	0.311	0.732	0.187	0.151
Calculated end-member fractions (mol %)											
Or	85.663	41.015	14.061	33.799	26.830	11.897	22.783	14.061	33.799	8.784	7.203
Ab	13.142	54.292	58.958	60.458	68.528	86.437	66.485	58.958	60.458	57.054	53.445
An	1.195	4.692	26.981	5.743	4.642	1.666	10.733	26.981	5.743	34.162	39.352
Rock type		Mafic dykes									
Major oxides (%)											
SiO_2	53.03	57.64	53.21	51.43	53.16	51.55	51.56	51.44	58.67	58.53	
TiO_2	0.09	0.03	0.08	0.02	0.04	0.02	0.05	0.03	0.01	0.05	
Al_2O_3	0.26	0.23	0.34	0.14	0.32	0.14	0.22	0.13	0.22	0.18	
FeO	27.39	24	27.11	29.87	30.07	30.07	30.32	29.94	24.04	23.8	
MnO	0.05	0.05	0	0.01	0.01	0	0	0.01	0	0.03	
MgO	0.1	0.03	0.13	0.1	0.09	0.01	0.072	0.04	0.01	0	
CaO	11.21	6.06	10.92	12.7	8.35	13.49	12.167	13.34	6.62	6.51	
Na_2O	6.26	7.92	6.47	5.16	5.57	5.16	5.259	5.39	8.33	8.17	
K_2O	0.77	2.46	0.77	0.87	3.3	0.4	1.368	0.43	2.76	2.75	
Total	99.16	98.44	99	100.36	100.93	100.9	101.04	100.78	100.68	100.05	
Calculated mineral formulae* (apfu)											
Si	2.139	2.342	2.150	2.050	2.107	2.044	2.041	2.042	2.331	2.340	
Ti	0.014	0.013	0.018	0.008	0.017	0.008	0.012	0.007	0.012	0.010	
Al	0.003	0.001	0.003	0.001	0.002	0.001	0.002	0.001	0.001	0.002	
Fe	2.210	1.950	2.190	2.381	2.383	2.384	2.401	2.377	1.911	1.903	
Mn	0.004	0.004	0.000	0.001	0.001	0.000	0.000	0.001	0.000	0.003	
Mg	0.008	0.003	0.010	0.008	0.007	0.001	0.006	0.003	0.001	0.000	
Ca	0.905	0.493	0.882	1.013	0.662	1.070	0.963	1.059	0.526	0.521	
Na	1.009	1.287	1.046	0.823	0.883	0.819	0.833	0.856	1.325	1.307	
K	0.125	0.400	0.122	0.139	0.523	0.065	0.217	0.070	0.439	0.441	

Table 1 (continued)

Rock type	Mafic dykes									
Major oxides (%)										
Calculated end-member fractions (mol %)										
Or	6.109	18.356	5.963	7.060	25.289	3.320	10.763	3.511	19.173	19.436
Ab	49.512	59.047	51.008	41.667	42.685	41.907	41.375	43.135	57.853	57.616
An	44.379	22.597	43.029	51.273	32.025	54.773	47.862	53.353	22.973	22.949
Rock type	Columnar jointed basalts									
Major oxides (%)										
SiO_2	53.25	52.98	53.61	52.49	53.39	52.89	53.57	54.12	53.36	52.98	56.02
TiO_2	0	0	0	0	0	0	0	0	0	0	0
Al_2O_3	30.02	29.93	30.1	30.25	29.69	30.01	29.95	29.33	29.07	29.19	28.01
FeO	0.65	0.64	0.55	0.45	0.69	0.58	0.41	0.34	0.81	0.9	0.57
MnO	0	0	0	0	0	0	0	0	0	0	0
MgO	0	0	0	0	0	0	0	0	0	0	0
CaO	12.02	11.89	11.83	12.32	12.16	12.14	11.67	11.45	11.62	11.96	9.87
Na2O	4.69	4.18	4.13	4.08	4.36	4.36	4.34	4.28	4.48	4.21	5.11
K2O	0.35	0.41	0.38	0.42	0.5	0.48	0.6	0.54	0.59	0.63	0.62
BaO	0.05	0.05	0.12	0.08	0.01	0.46	0.21	0.22	0.09	0.17	0.03
Total	101.03	100.06	100.72	100.09	100.82	100.46	100.54	100.06	99.94	99.90	100.23
Calculated mineral formulae* (apfu)										
Si	2.108	2.118	2.129	2.098	2.118	2.106	2.131	2.164	2.136	2.121	2.236
Al	1.585	1.595	1.594	1.612	1.571	1.593	1.589	1.563	1.551	1.558	1.490
Ti	0.000	0.000	0.000	0.000	0.000	0.000	0.000	0.000	0.000	0.000	0.000
Fe	0.051	0.051	0.044	0.036	0.055	0.046	0.033	0.027	0.065	0.072	0.045
Mg	0.000	0.000	0.000	0.000	0.000	0.000	0.000	0.000	0.000	0.000	0.000
Ca	0.952	0.951	0.940	0.985	0.965	0.967	0.929	0.915	0.930	0.958	0.788
Na	0.743	0.668	0.656	0.652	0.692	0.694	0.691	0.684	0.717	0.674	0.816
K	0.055	0.066	0.060	0.067	0.079	0.076	0.095	0.086	0.094	0.101	0.099
Ba	0.004	0.004	0.010	0.006	0.001	0.037	0.017	0.018	0.007	0.014	0.002
Calculated end-member fractions (mol %)										
Or	3.167	3.892	3.645	3.940	4.570	4.400	5.568	5.121	5.423	5.823	5.813
Ab	42.443	39.677	39.616	38.274	39.854	39.963	40.278	40.588	41.176	38.909	47.914
An	54.389	56.431	56.739	57.786	55.576	55.637	54.153	54.291	53.401	55.268	46.273
Rock type	Columnar jointed basalts									
Major oxides (%)										
SiO_2	54.58	53.99	52.451	52.83	56.99	51.91	60.36	60.1	51.63	61.13	53.11
TiO_2	0	0	0	0	0	0	0	0	0	0	0
Al_2O_3	27.89	29.21	31.06	29.94	21.06	30.48	20.51	24.95	26.96	22.01	30.02
FeO	0.69	0.61	0.36	0.39	0.63	0.69	0.61	0.53	0.44	0.42	0.72
MnO	0	0	0	0	0	0	0	0	0	0	0
MgO	0	0	0	0	0	0	0	0	0	0	0
CaO	10.97	12.03	12.01	12.23	10.79	11.29	10.03	6.78	9.25	0.63	11.71
Na2O	4.87	4.22	4.07	3.95	8.26	4.54	4.71	5.96	5.01	4.38	4.01
K2O	0.69	0.44	0.6	0.55	2.92	0.68	1.45	2.26	0.68	8.3	0.52
BaO	0.40	0.01	0.18	0.18	0.07	0.62	2.64	0.27	8	3.64	0.04
Total	99.70	100.51	100.55	99.92	100.72	99.62	97.68	100.58	101.97	96.87	100.13
Calculated mineral formulae* (apfu)										
Si	2.190	2.149	2.087	2.115	2.263	2.084	2.472	2.390	2.025	2.524	2.122

Table 1 (continued)

Rock type	Columnar jointed basalts										
Major oxides (%)											
Al	1.492	1.550	1.647	1.598	1.115	1.632	1.120	1.323	1.410	1.212	1.599
Ti	0.000	0.000	0.000	0.000	0.000	0.000	0.000	0.000	0.000	0.000	0.000
Fe	0.055	0.049	0.029	0.031	0.050	0.055	0.050	0.042	0.035	0.035	0.058
Mg	0.000	0.000	0.000	0.000	0.000	0.000	0.000	0.000	0.000	0.000	0.000
Ca	0.880	0.958	0.956	0.979	0.857	0.907	0.821	0.539	0.726	0.052	0.936
Na	0.782	0.672	0.648	0.632	1.312	0.729	0.772	0.948	0.786	0.723	0.641
K	0.111	0.070	0.095	0.088	0.464	0.109	0.238	0.360	0.107	1.371	0.083
Ba	0.032	0.001	0.014	0.014	0.006	0.050	0.216	0.021	0.628	0.301	0.003
Calculated end-member fractions (mol %)											
Or	6.247	4.122	5.621	5.181	17.617	6.259	12.975	19.466	6.592	63.871	5.007
Ab	44.092	39.532	38.126	37.211	49.834	41.786	42.148	51.335	48.570	33.705	38.613
An	49.660	56.347	56.253	57.607	32.549	51.956	44.877	29.199	44.838	2.424	56.379

* Calculated based on 8 oxygen atoms per formula unit

the respective pressure of 2 to 13 kbar for the columnar jointed basalts and 4 to 12 kbar for the mafic dykes. This wide range of pressure corresponds to a wide range of clinopyroxene crystallization depth as mostly founded in mafic intrusions of the Cameroun Volcanic Line [36].

Moreover, the feldspar triangular thermometry diagram [37] gives the temperature ranging from 700 to 1000 °C for the mafic dykes and from 800 to 1100 °C for the columnar jointed basalts with one sample exceeding 1100 °C (Fig. 6d).

Evaluating the oxygen fugacity of the magma of the studied mafic rocks is important because oxygen fugacity plays an essential role in changing the liquidus temperature, melt and crystals composition, and the magmatic processes in general [38]. Plotted on the $Al^{VI} + 2Ti + Cr$ versus $Al^{VI} + Na$ diagram [39], the studied samples fall in the high oxygen fugacity area (Fig. 7).

4.5 Geochemistry

4.5.1 Columnar jointed basalts

The columnar jointed basalts are basic to intermediate and present low to moderate content of SiO_2 (46.89–52.71 wt.%) (Table 3). They plot in the basalt, trachy-basalt and basaltic trachy-andesite field of the TAS (total alkali-silica) classification diagram after Lebas et al. [40] (Fig. 8a). They display moderate to high Al_2O_3 (12.25–15.85wt.%), TiO_2 (1.69–2.29 wt.%) and low MgO (4.15–7.9 wt%) contents. The columnar jointed basalts present low to moderate Mg# value (40.16–53.05) and the A/CNK molar ratio ranging from 0.75 to 1.41. The LOI (1–6 wt.%) of the studied columnar jointed basalts are low to high, testifying to the variable degree of weathering of the rock. All the columnar jointed basalts samples plot within the Calc-alkaline domain on the AFM diagram of Irvine and Baragar [41] (Fig. 8b). On the plot of SiO_2 (wt%) versus other major and trace elements, Al_2O_3 and K_2O show a positive correlation with SiO_2 while

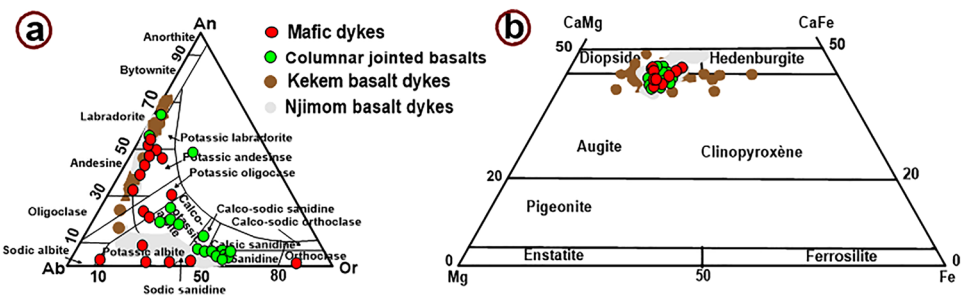

Fig. 5 **a** Feldspar composition for the Mfengou-Manki mafic rocks plotted on the An-Ab-Or diagram [88], **b** Pyroxene composition of the studied rocks on a Wo–En–Fs diagram [31]

Table 2 Representative chemical composition (wt%) and structural formulae of clinopyroxenes from the Mfengou-Manki mafic rocks

Rock type	Mafic dykes								
SiO_2	51.02	49.64	50.45	50.41	50.08	49.07	49.01	48.42	49.57
TiO_2	1.15	0.18	0.08	1.31	0.97	1.24	1.92	2.45	0.78
Al_2O_3	2.98	2.33	3.02	4.17	2.71	4.27	4.07	4.86	3.97
Cr_2O_3	0.14	0.21	0.25	0.13	0.09	0.14	0.24	0.15	0.32
FeO_{tot}	10.03	17.98	17.12	10.01	12.25	12.45	11.78	10.07	11.31
MnO	0.31	0.98	0.87	0.42	1.12	1.01	0.34	0.12	0.19
MgO	12.32	8.92	8.02	12.07	11.85	10.41	12.14	12.34	13.08
CaO	21.86	21.16	21.98	21.05	21.25	20.97	20.18	20.51	19.81
Na_2O	0.52	0.83	0.78	0.51	0.41	0.49	0.49	0.34	0.31
K_2O	0.00	0.00	0.00	0.00	0.00	0.00	0.00	0.00	0.00
Total	100.33	102.23	102.32	100.08	100.73	100.05	100.17	99.11	99.02
Si	1.908	1.871	1.898	1.889	1.881	1.863	1.845	1.833	1.870
Al^{iv}	0.092	0.103	0.102	0.111	0.119	0.137	0.155	0.167	0.130
Al^{vi}	0.039	0.000	0.032	0.074	0.001	0.054	0.026	0.050	0.046
Ti	0.032	0.005	0.002	0.037	0.027	0.035	0.054	0.070	0.022
Cr	0.004	0.006	0.007	0.004	0.003	0.004	0.007	0.004	0.010
Fe^{3+}	0.021	0.199	0.116	0.000	0.090	0.044	0.049	0.000	0.052
Fe^{2+}	0.292	0.368	0.423	0.314	0.294	0.352	0.322	0.319	0.304
Mn	0.010	0.031	0.028	0.013	0.036	0.032	0.011	0.004	0.006
Mg	0.687	0.501	0.450	0.674	0.664	0.589	0.681	0.696	0.736
Ca	0.876	0.854	0.886	0.845	0.855	0.853	0.814	0.832	0.801
Na	0.038	0.061	0.057	0.037	0.030	0.036	0.036	0.025	0.023
K	0.000	0.000	0.000	0.000	0.000	0.000	0.000	0.000	0.000
Wo	46.44	43.74	46.58	45.77	44.10	45.62	43.37	44.94	42.16
En	36.41	25.65	23.65	36.52	34.22	31.51	36.30	37.62	38.73
Fs	17.15	30.61	29.77	17.71	21.68	22.88	20.34	17.43	19.11
T (°C)[(a)]	1175	1110	1091	1196	1180	1163	1171	1171	1233
Rock type	Columnar jointed basalts								
SiO_2	47.64	47.48	47.58	47.86	46.78	46.12	45.31	47.01	47.64	47.48
TiO_2	2.45	3.27	1.62	1.62	2.34	2.46	3.65	2.42	2.45	3.27
Al_2O_3	4.11	5.78	4.53	5.21	5.87	5.94	6.52	5.16	4.11	5.78
Cr_2O_3	0.12	0.15	0.12	0.08	0.12	0.21	0.54	0.51	0.12	0.15
FeO_{tot}	11.32	10.45	12.08	12.18	10.44	10.97	10.23	10.22	11.32	10.45
MnO	0.35	0.12	0.47	0.64	0.35	0.45	0.27	0.43	0.35	0.12
MgO	12.47	11.97	11.45	11.75	12.89	12.87	12.31	12.45	12.47	11.97
CaO	20.65	21.43	21.03	21.01	20.38	20.19	20.13	20.35	20.65	21.43
Na_2O	0.62	0.61	0.84	0.52	0.51	0.59	0.62	0.53	0.62	0.61
K_2O	0.00	0.00	0.00	0.00	0.00	0.00	0.00	0.00	0.00	0.00
Total	99.73	101.26	99.72	100.35	99.68	99.80	99.58	99.08	99.73	101.26
Si	1.796	1.763	1.796	1.788	1.755	1.730	1.709	1.780	1.796	1.763
Al^{iv}	0.183	0.237	0.202	0.212	0.245	0.263	0.290	0.220	0.183	0.237
Al^{vi}	0.000	0.016	0.000	0.018	0.015	0.000	0.000	0.011	0.000	0.016
Ti	0.069	0.091	0.046	0.046	0.066	0.069	0.104	0.069	0.069	0.091
Cr	0.004	0.004	0.004	0.002	0.004	0.006	0.016	0.015	0.004	0.004
Fe^{3+}	0.128	0.077	0.172	0.138	0.132	0.176	0.115	0.095	0.128	0.077
Fe^{2+}	0.229	0.248	0.209	0.243	0.196	0.168	0.207	0.229	0.229	0.248
Mn	0.011	0.004	0.015	0.020	0.011	0.014	0.009	0.014	0.011	0.004
Mg	0.701	0.663	0.644	0.655	0.721	0.720	0.692	0.703	0.701	0.663
Ca	0.834	0.853	0.851	0.841	0.819	0.811	0.813	0.826	0.834	0.853

Table 2 (continued)

Rock type	Columnar jointed basalts									
Na	0.045	0.044	0.061	0.038	0.037	0.043	0.045	0.039	0.045	0.044
K	0.000	0.000	0.000	0.000	0.000	0.000	0.000	0.000	0.000	0.000
Wo	43.83	46.25	44.97	44.35	43.60	42.94	44.28	44.25	43.83	46.25
En	36.83	35.94	34.07	34.51	38.37	38.09	37.68	37.67	36.83	35.94
Fs	19.34	17.81	20.96	21.14	18.03	18.97	18.04	18.08	19.34	17.81
T (°C)[(a)]	1142	1120	1138	1169	1178	1169	1133	1169	1142	1120
Rock type	Columnar jointed basalts									
SiO_2	47.64	47.48	47.64	47.48	47.58	47.64	47.48	47.58	47.86	46.78
TiO_2	2.45	3.27	2.45	3.27	1.62	2.45	3.27	1.62	1.62	2.34
Al_2O_3	4.11	5.78	4.11	5.78	4.53	4.11	5.78	4.53	5.21	5.87
Cr_2O_3	0.12	0.15	0.12	0.15	0.12	0.12	0.15	0.12	0.08	0.12
FeO_{tot}	11.32	10.45	11.32	10.45	12.08	11.32	10.45	12.08	12.18	10.44
MnO	0.35	0.12	0.35	0.12	0.47	0.35	0.12	0.47	0.64	0.35
MgO	12.47	11.97	12.47	11.97	11.45	12.47	11.97	11.45	11.75	12.89
CaO	20.65	21.43	20.65	21.43	21.03	20.65	21.43	21.03	21.01	20.38
Na_2O	0.62	0.61	0.62	0.61	0.84	0.62	0.61	0.84	0.52	0.51
K_2O	0.00	0.00	0.00	0.00	0.00	0.00	0.00	0.00	0.00	0.00
Total	99.73	101.26	99.73	101.26	99.72	99.73	101.26	99.72	100.35	99.68
Si	1.796	1.763	1.796	1.763	1.796	1.796	1.763	1.796	1.788	1.755
Al^{iv}	0.183	0.237	0.183	0.237	0.202	0.183	0.237	0.202	0.212	0.245
Al^{vi}	0.000	0.016	0.000	0.016	0.000	0.000	0.016	0.000	0.018	0.015
Ti	0.069	0.091	0.069	0.091	0.046	0.069	0.091	0.046	0.046	0.066
Cr	0.004	0.004	0.004	0.004	0.004	0.004	0.004	0.004	0.002	0.004
Fe^{3+}	0.128	0.077	0.128	0.077	0.172	0.128	0.077	0.172	0.138	0.132
Fe^{2+}	0.229	0.248	0.229	0.248	0.209	0.229	0.248	0.209	0.243	0.196
Mn	0.011	0.004	0.011	0.004	0.015	0.011	0.004	0.015	0.020	0.011
Mg	0.701	0.663	0.701	0.663	0.644	0.701	0.663	0.644	0.655	0.721
Ca	0.834	0.853	0.834	0.853	0.851	0.834	0.853	0.851	0.841	0.819
Na	0.045	0.044	0.045	0.044	0.061	0.045	0.044	0.061	0.038	0.037
K	0.000	0.000	0.000	0.000	0.000	0.000	0.000	0.000	0.000	0.000
Wo	43.831	46.249	43.831	46.249	44.972	43.831	46.249	44.972	44.351	43.602
En	36.828	35.944	36.828	35.944	34.069	36.828	35.944	34.069	34.512	38.372
Fs	19.342	17.808	19.342	17.808	20.958	19.342	17.808	20.958	21.137	18.026
T (°C)[(a)]	1142	1120	1142	1120	1138	1142	1120	1138	1169	1178
Rock type	Columnar jointed basalts									
SiO_2	46.12	45.31	47.01	47.29	48.11	47.85	49.78	49.22	48.23	49.13
TiO_2	2.46	3.65	2.42	2.35	1.93	1.71	0.97	2.07	2.25	1.45
Al_2O_3	5.94	6.52	5.16	5.79	5.06	5.53	4.66	4.24	5.35	3.41
Cr_2O_3	0.21	0.54	0.51	0.21	0.25	0.07	0.14	0.14	0.15	0.17
FeO_{tot}	10.97	10.23	10.22	11.07	11.11	11.08	10.87	11.53	10.57	10.31
MnO	0.45	0.27	0.43	0.18	0.49	0.43	0.31	0.29	0.52	0.62
MgO	12.87	12.31	12.45	11.88	12.24	11.87	12.97	12.57	11.67	12.45
CaO	20.19	20.13	20.35	19.89	19.92	20.17	19.78	20.82	21.86	21.23
Na_2O	0.59	0.62	0.53	0.57	0.54	0.51	0.48	0.34	0.51	0.51
K_2O	0.00	0.00	0.00	0.00	0.00	0.00	0.00	0.00	0.00	0.00
Total	99.80	99.58	99.08	99.23	99.65	99.22	99.96	101.08	101.11	99.28
Si	1.730	1.709	1.780	1.792	1.814	1.812	1.862	1.832	1.796	1.857
Al^{iv}	0.263	0.290	0.220	0.208	0.186	0.188	0.138	0.168	0.204	0.143

Table 2 (continued)

Rock type	Columnar jointed basalts									
Al^{vi}	0.000	0.000	0.011	0.050	0.039	0.059	0.068	0.018	0.030	0.009
Ti	0.069	0.104	0.069	0.067	0.055	0.049	0.027	0.058	0.063	0.041
Cr	0.006	0.016	0.015	0.006	0.007	0.002	0.004	0.004	0.004	0.005
Fe^{3+}	0.176	0.115	0.095	0.060	0.069	0.067	0.046	0.055	0.080	0.084
Fe^{2+}	0.168	0.207	0.229	0.291	0.281	0.283	0.294	0.304	0.249	0.242
Mn	0.014	0.009	0.014	0.006	0.016	0.014	0.010	0.009	0.016	0.020
Mg	0.720	0.692	0.703	0.671	0.688	0.670	0.723	0.697	0.648	0.702
Ca	0.811	0.813	0.826	0.807	0.805	0.818	0.793	0.830	0.872	0.860
Na	0.043	0.045	0.039	0.042	0.039	0.037	0.035	0.025	0.037	0.037
K	0.000	0.000	0.000	0.000	0.000	0.000	0.000	0.000	0.000	0.000
Wo	42.943	44.284	44.249	44.002	43.295	44.161	42.486	43.796	46.750	45.083
En	38.088	37.680	37.667	36.568	37.015	36.160	38.763	36.791	34.726	36.786
Fs	18.969	18.036	18.085	19.430	19.690	19.679	18.751	19.414	18.524	18.130
T (°C)[(a)]	1169	1133	1169	1166	1184	1187	1229	1172	1143	1178

Rock type	Columnar jointed basalts		
SiO_2	48.83	47.83	48.09
TiO_2	1.78	1.43	2.81
Al_2O_3	4.08	4.91	3.98
Cr_2O_3	0.17	0.54	0.42
FeO_{tot}	11.45	11.58	10.54
MnO	0.23	0.35	0.21
MgO	11.75	11.98	12.74
CaO	20.57	20.01	20.33
Na_2O	0.53	0.61	0.69
K_2O	0.00	0.00	0.00
Total	99.39	99.24	99.81
Si	1.852	1.812	1.809
Al^{iv}	0.148	0.188	0.176
Al^{vi}	0.034	0.031	0.000
Ti	0.051	0.041	0.079
Cr	0.005	0.016	0.012
Fe^{3+}	0.046	0.104	0.084
Fe^{2+}	0.317	0.263	0.247
Mn	0.007	0.011	0.007
Mg	0.664	0.677	0.714
Ca	0.836	0.812	0.819
Na	0.039	0.045	0.050
K	0.000	0.000	0.000
Wo	44.681	43.505	43.768
En	35.512	36.241	38.163
Fs	19.808	20.253	18.069
T (°C)[a]	1165	1191	1143

[a]Temperature calculated after Nimis and Taylor [28]

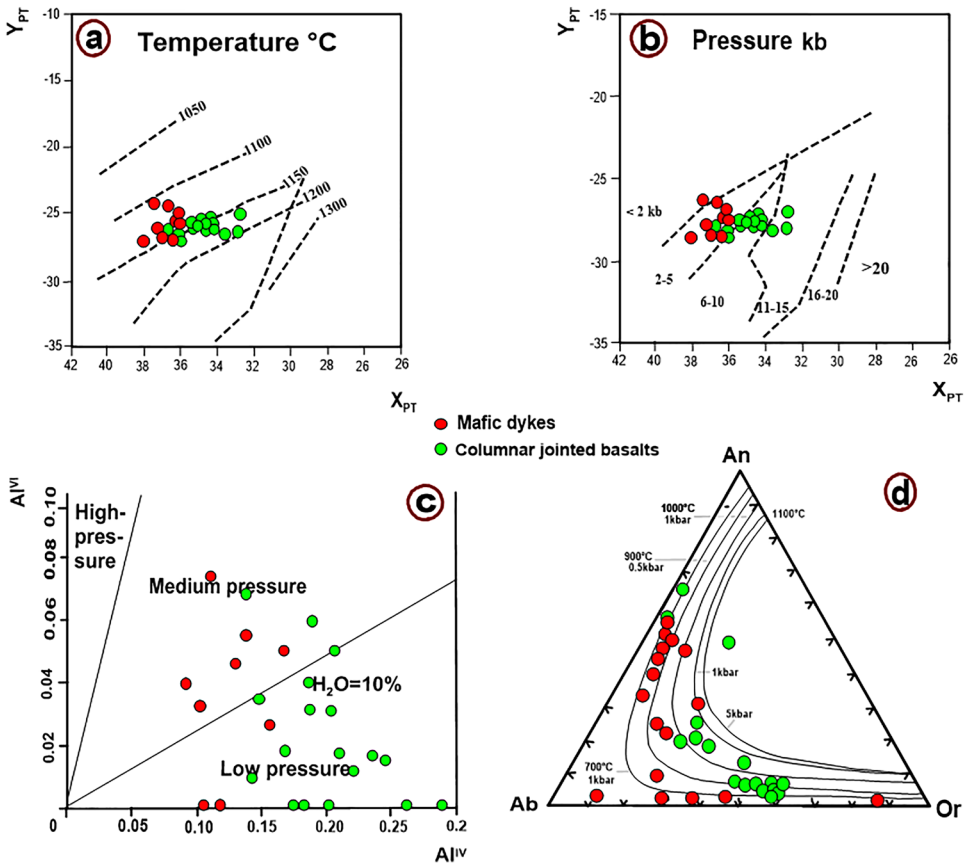

Fig. 6 **a** Crystallization temperature of pyroxenes of the studied mafic rocks [32], (**b**) Estimated pressure of the crystallization of the pyroxenes using the diagram after Soesoo [32], **c** Clinopyroxene barometry diagram [34] of the studied mafic rocks, **d** Temperature of crystallization of the feldspars of the Mfengou-Manki mafic rocks using the triangular thermometry diagram after Kroll et al. [37]

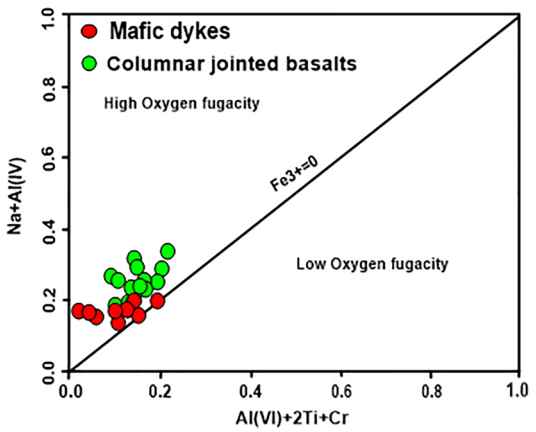

Fig. 7 Oxygen fugacity of the studied mafic rocks using the $Al^{VI}+2Ti+Cr$ versus $Al.^{VI}+Na$ diagram after Schweitzer et al. [39]

MgO, CaO and TiO_2 display a negative correlation with SiO_2 (Fig. 9). The trace elements such as Ni and Cr present negative correlation with SiO_2 while Y and Ba present positive correlation with SiO_2 (Fig. 9).

The studied columnar jointed basalts show low concentrations of Ni (35- 173 ppm) and low to moderate concentrations of Cr (87–268 ppm) and Co (29–53 ppm). On the multi-element diagram normalized to primitive mantle abundances given by McDonough and Sun [42], the columnar jointed basalts display slight depletion in Nb and Ta, pronounced depletion in Th, U, Pb and Zr, and enrichment in Cs, Ba and Rb (Fig. 10a). The REE diagram normalized to the primitive mantle [42] shows enrichment in LREE ($La_N/Sm_N = 2.39–3.65$) compared to HREE ($Gd_N/Yb_N = 1.80–2.94$) and negative to slight positive europium anomalies ($(Eu/Eu^*)_N = 0.6$ to 1.03) (Fig. 10b).

Table 3 Major (wt%) and trace (ppm) element contents in mafic columnar joints and mafic dykes from the Mfengou-Manki area

Rocks types	Columnar jointed basalts							
Sample n°	MF1	MF2	MF3	MF4	MF5	MF6	MF7	MF8
SiO_2	49.33	50.61	47.42	48.57	47.53	46.95	47.36	46.89
Al_2O_3	15.12	15.98	15.02	15.03	15.01	15.06	15.17	14.97
Fe_2O_3tot	11.34	11.02	10.91	11.23	10.98	11.02	10.97	11.25
MnO	0.15	0.13	0.15	0.14	0.16	0.15	0.15	0.17
MgO	4.28	4.15	5.28	6.31	5.94	6.3	6.25	6.4
CaO	6.85	7.02	7.38	6.53	7.17	6.36	6.39	7.07
Na_2O	2.75	2.31	2.83	3.04	3.19	3.25	3.03	3.16
K_2O	3.11	2.88	2.13	1.89	1.98	1.96	1.87	1.83
TiO_2	1.81	1.83	1.89	1.7	1.93	1.88	1.91	1.9
$P2O_5$	0.74	0.59	0.53	0.51	0.58	0.55	0.61	0.59
LOI	3.54	4.02	5.95	4.35	4.59	5.59	4.62	4.16
Total	99.02	100.54	99.49	99.3	99.06	99.07	98.33	98.39
Sc	18.15	17.83	16.98	18.05	17.59	16.99	17.25	18.33
V	123.12	128.45	148.79	146.51	150.32	149.09	152.67	155.34
Cr	87.61	91.03	169.13	170.08	169.4	170.03	179.07	165.79
Co	36.28	30.21	37.42	40.01	39.54	38.98	39.74	39.23
Ni	35.6	43.11	94.38	103.45	98.51	109.34	100.07	102.84
Cu	49.89	45.61	50.13	49.31	48.12	51.62	59.54	51.02
Zn	110.28	98.851	101.2	92.18	99.68	86.47	99.13	94.2
Ga	19.75	21.06	18.01	17.32	18.01	16.89	19.21	18.14
Rb	89.34	103.21	51.37	53.88	52.75	49.03	48.11	55.07
Sr	498.79	435.04	427.78	475.24	506.23	515.41	492.32	496.41
Y	36.42	35.23	30.12	27.35	28.75	28.02	27.12	30.15
Zr	298.03	278.45	213.12	217.21	221.14	210.61	223.41	218.04
Nb	49.31	39.11	28.11	27.81	28.03	28.31	27.18	27.33
Cs	1.45	2.63	1.52	1.22	1.32	1.08	0.97	1.02
Ba	803.23	953.22	502.31	611.5	697.24	719.31	672.48	594.32
La	51.36	49.36	32.04	30.64	31.19	30.13	31.05	30.42
Ce	109.74	102.14	67.41	64.92	68.37	64.59	67.42	66.17
Pr	10.99	12.61	8.39	7.33	8.71	7.97	8.05	8.27
Nd	47.38	46.53	32.47	32.06	34.31	32.85	32.97	32.97
Sm	8.79	8.94	7.01	6.98	7.58	6.75	7.09	7.03
Eu	2.17	2.11	1.85	1.81	1.72	1.98	1.77	2.01
Gd	8.45	8.07	7.03	6.48	7.04	6.34	6.45	7.09
Tb	1.14	1.04	1.08	1.03	0.95	1.01	1.04	1.12
Dy	6.93	6.75	5.51	5.03	6.13	5.75	5.72	5.98
Ho	1.27	1.24	1.22	1.09	1.21	1.15	1.13	1.11
Er	3.75	3.45	3.17	3.08	3.13	2.95	3.12	3.08
Tm	0.49	0.49	0.44	0.48	0.47	0.43	0.41	0.43
Yb	3.21	3.12	2.75	2.92	3.02	2.63	2.96	2.89
Lu	0.52	0.46	0.38	0.41	0.43	0.41	0.42	0.44
Hf	5.98	6.01	5.01	4.47	4.75	4.57	4.95	4.67
Ta	2.75	2.38	1.85	1.73	1.89	1.91	1.87	1.78
Pb	6.83	7.01	4.79	4.35	4.25	4.23	4.21	4.99
Th	4.75	6.3	2.49	2.58	2.76	2.57	2.62	2.58
U	1.52	1.37	0.58	0.66	0.72	0.63	0.58	0.69
Mg#	40.22	40.16	46.31	50.04	49.09	50.47	50.38	50.35
$(Eu/Eu^*)_N$	0.77	0.75	0.80	0.82	0.72	0.92	0.80	0.87

Table 3 (continued)

Rock type	Columnar jointed basalts								
Sample n°	MF9	MF10	MF11	MF12	MF13	DF1	DF2	DF3	DF4
SiO_2	50.23	50.04	51.13	47.28	46.98	48.74	51.99	48.35	52.71
Al_2O_3	15.85	14.78	15.01	12.25	14.45	16.52	15.67	15.45	15.78
Fe_2O_3tot	10.16	10.2	9.87	11.58	10.94	11.34	10.52	12.01	10.35
MnO	0.17	0.15	0.14	0.19	0.15	0.17	0.15	0.18	0.16
MgO	5.39	4.87	4.35	5.27	6.08	7.19	4.62	6.83	4.64
CaO	5.43	7.19	6.79	11.98	11.95	8.01	6.88	7.64	6.49
Na_2O	3.08	2.75	2.52	2.37	2.79	2.78	2.52	3.08	3.42
K_2O	2.67	2.87	2.85	1.93	1.08	2.81	3.32	2.12	3.01
TiO_2	1.87	1.69	1.59	2.04	2.29	1.93	1.87	2.04	1.87
P_2O_5	0.58	0.54	0.56	0.41	0.4	0.45	0.63	0.61	0.62
LOI	4.54	4.35	4.59	4.21	3.06	1.83	2.41	1.87	1.72
Total	99.97	99.43	99.4	99.51	100.17	101.77	100.58	100.18	100.77
Sc	16.87	18.78	17.08	16.97	18.45	18.21	17.32	18.15	18.58
V	119.11	123.18	117.28	203.87	212.67	151.45	105.12	142.28	107.13
Cr	101.01	99.47	95.32	243.12	268.23	161.23	89.35	156.21	92.03
Co	31.08	30.45	29.45	50.95	53.68	42.97	36.78	42.31	36.79
Ni	64.14	51.28	43.16	211.02	173.47	137.28	65.34	124.12	65.96
Cu	49.12	41.65	43.44	59.6	70.73	76.26	79.12	68.27	75.86
Zn	111.21	100.34	98.58	112.6	121.81	74.38	83.11	85.62	83.12
Ga	21.31	19.12	20.78	18.96	20.13	16.85	17.85	20.01	17.19
Rb	93.23	95.31	96.32	19.28	23.17	105.34	238.25	59.11	204.86
Sr	450.41	486.34	469.45	678.83	608.75	687.33	937.85	571.28	795.41
Y	32.46	30.89	31.69	19.03	21.45	32.71	54.35	32.11	58.33
Zr	285.98	253.18	250.45	132.11	129.24	311.21	154.28	204.06	189.03
Nb	39.12	35.45	34.99	27.24	28.67	33.54	30.72	32.45	24.73
Cs	2.32	3.79	3.94	2.38	3.65	2.58	3.07	1.04	2.36
Ba	786.34	740.59	735.48	278.31	265.28	591.31	694.28	607.45	689.15
La	47.78	52.83	51.63	20.13	22.85	25.31	33.78	27.44	42.16
Ce	100.11	107.31	103.28	39.15	44.78	55.31	72.89	61.03	85.14
Pr	12.9	12.47	12.35	5.63	5.86	6.12	8.42	7.43	9.76
Nd	46.34	47.78	46.19	19.45	22.19	24.6	34.16	31.78	39.44
Sm	8.97	9.71	9.23	5.27	5.39	4.67	6.21	6.3	7.38
Eu	1.85	1.99	1.79	1.68	1.69	1.38	1.41	1.78	1.59
Gd	7.89	7.98	7.91	4.61	5.33	4.97	6.01	6.52	6.87
Tb	1.19	1.20	1.19	0.83	0.85	0.68	0.75	0.91	0.89
Dy	6.78	7.15	7.14	4.05	4.47	3.69	4.03	4.98	5.01
Ho	1.37	1.41	1.38	0.75	0.83	0.72	0.75	0.89	0.91
Er	3.49	3.07	3.65	2.13	2.21	2.12	2.11	2.56	2.42
Tm	0.46	0.52	0.53	0.29	0.31	0.28	0.27	0.34	0.35
Yb	3.14	3.39	3.27	1.98	1.85	1.86	1.69	2.19	2.14
Lu	0.51	0.52	0.51	0.27	0.26	0.27	0.26	0.32	0.33
Hf	5.38	5.99	6.01	2.95	2.91	7.74	3.89	5.07	4.59
Ta	2.68	2.78	2.79	1.87	1.75	1.87	1.69	1.74	1.13
Pb	5.84	5.77	5.31	5.44	5.23	2.58	3.07	2.69	3.78
Th	6.45	8.95	9.01	2.13	2.25	1.86	2.69	1.79	3.31
U	1.45	1.73	1.78	0.59	0.62	0.45	0.51	0.43	0.62
Mg#	48.60	45.98	44.00	44.79	49.76	53.05	43.91	50.34	44.42
$(Eu/Eu^*)_N$	0.67	0.69	0.64	1.04	0.96	0.87	0.70	0.84	0.68

Table 3 (continued)

Rock type	Mafic dykes						
Sample n°	DB1	DB2	DG4	DG5	DB6	DG7	DBI 9
SiO_2	46.83	46.22	50.16	50.44	47.1	49.9	46.23
Al_2O_3	12.11	11.45	14.24	14.1	13.96	13.61	13.41
Fe_2O_3tot	12.01	12.12	11.93	11.92	12.63	13.25	12.09
MnO	0.13	0.14	0.12	0.12	0.13	0.15	0.18
MgO	12.78	11.85	8.02	8	11.67	8.09	7.02
CaO	11.37	11.5	6.78	6.78	8.4	5.25	9.16
Na_2O	1.82	2.14	2.47	2.75	2.4	2.51	2.62
K_2O	0.24	1.2	2.8	2.78	1.74	4.31	1.05
TiO_2	2.33	2.64	1.97	1.98	2.03	1.81	2.18
P_2O_5	0.22	0.27	0.39	0.44	0.49	0.57	0.35
LOI	7.308	4.158	2.829	3.298	3.34	2.721	5.44
Total	107.148	103.688	101.709	102.608	103.89	102.171	99.73
Sc	18.86	16.86	16.97	16.29	18.13	16.52	17.67
V	183.15	168.79	111.40	104.58	117.37	88.99	204.96
Cr	274.99	295.44	152.97	147.50	171.65	133.68	281.03
Co	45.78	49.67	29.50	28.55	34.23	29.54	5268
Ni	198.51	240.09	96.82	95.49	120.92	86.58	229.45
Cu	76.86	80.26	61.20	66.04	59.18	63.80	61.6
Zn	85.25	87.01	83.04	96.63	79.40	85.28	101.37
Ga	14.92	15.60	17.27	17.16	13.61	16.07	18.01
Rb	16.07	2.65	64.59	70.11	29.99	59.33	22.45
Sr	491.81	301.55	420.91	396.10	398.41	523.37	541.96
Y	19.46	18.75	34.04	34.02	26.67	29.36	18.12
Zr	73.89	64.24	142.49	141.58	113.50	150.37	125.46
Nb	25.81	17.16	43.39	41.06	26.95	58.64	26.13
Cs	1.88	1.94	0.79	1.02	0.57	0.17	4.09
Ba	243.99	91.20	683.66	622.82	532.83	954.88	258.34
La	15.68	10.99	41.26	40.42	22.83	38.58	19.71
Ce	30.24	21.39	82.33	80.84	47.31	75.37	37.73
Pr	3.41	2.50	8.80	8.72	5.36	8.09	4.98
Nd	14.88	11.44	34.69	34.70	22.37	31.52	19.21
Sm	4.05	3.32	8.03	8.17	5.70	7.14	4.72
Eu	1.34	1.18	1.88	1.87	1.61	2.16	1.31
Gd	3.93	3.48	6.77	6.72	4.96	5.89	4.65
Tb	0.55	0.52	0.93	0.91	0.70	0.79	0.75
Dy	3.46	3.23	5.75	5.60	4.50	4.93	3.97
Ho	0.65	0.60	1.09	1.09	0.87	0.95	0.73
Er	1.60	1.48	2.81	2.85	2.18	2.48	1.95
Tm	0.24	0.22	0.42	0.43	0.33	0.37	0.29
Yb	1.61	1.48	2.83	2.86	2.19	2.49	1.75
Lu	0.24	0.22	0.41	0.42	0.32	0.36	0.24
Hf	1.89	1.86	3.87	3.84	2.93	3.84	2.85
Ta	5.09	6.07	13.74	9.72	14.06	19.60	1.63
Pb	10.87	4.06	8.51	10.35	5.81	6.98	4.77
Th	1.39	0.92	5.09	4.62	1.56	2.75	2.13
U	0.25	0.15	0.58	0.56	0.24	0.51	0.57
Mg#	65.48	63.54	54.51	54.47	62.22	52.11	50.86
$(Eu/Eu^*)_N$	1.02	1.05	0.77	0.77	0.92	1.01	0.85

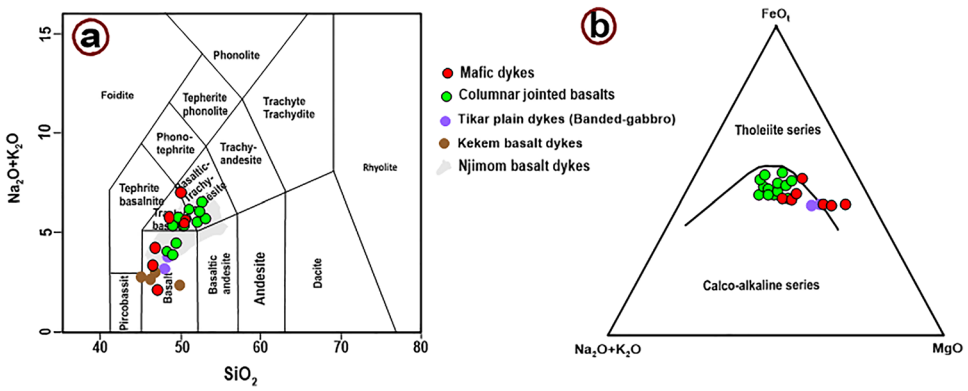

Fig. 8 **a** Classification diagram of the Mfengou-Manki mafic rocks after Le Bas et al. [40], **b** AFM diagram of the studied mafic rocks after Irvigne and Baragar [41]

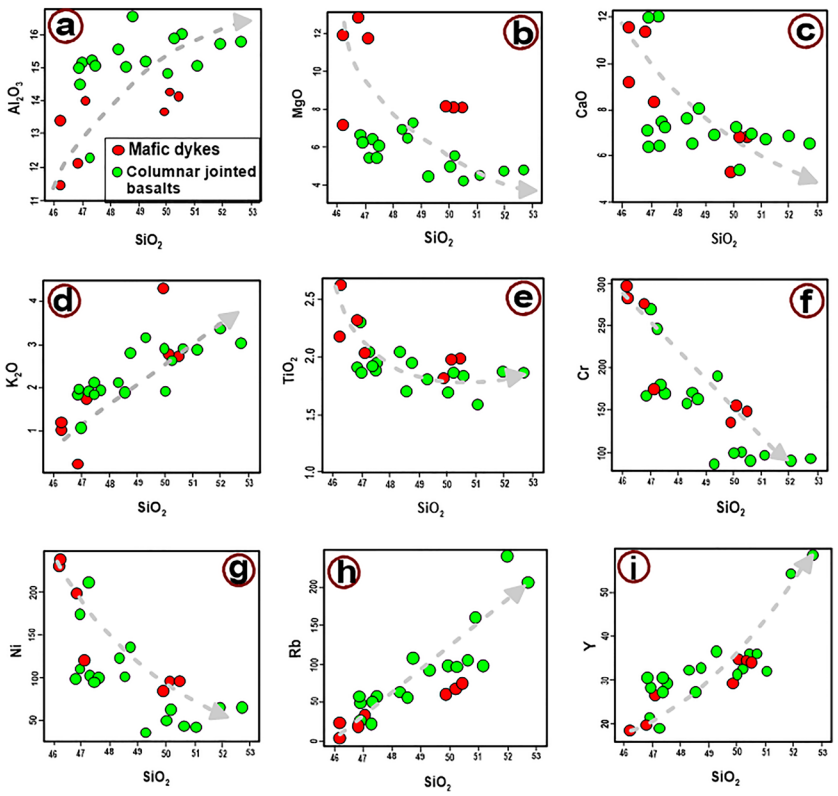

Fig. 9 Harker diagram of some major and trace elements of the studied mafic rocks against SiO_2

4.5.2 Mafic dykes

The mafic dykes are essentially basic, with a narrow SiO_2 content ranging from 46.89 wt% to 50.44 wt%. Plotted on the TAS (total alkali silica) classification diagram after Lebas et al. [40], the mafic dyke samples fall in the field of basalt, trachy-basalt and basaltic trachy-andesite (Fig. 8a). They present high MgO (8–12.85 wt.%) and TiO_2 (1.87–2.64 wt.%) with moderate to high Mg# (50–65) and the A/CNK molar ratio varying from 0.77–1.18. The mafic dykes display a wide range of LOI values (2.89–7.30 wt.%) (Table 3). On the AFM diagram after Irvine and Baragar [41], they plot on the calc-alkaline fields (Fig. 8b). Plotted on the SiO_2 versus other major and trace elements variation diagrams, Al_2O_3, and K_2O present a positive correlation with SiO_2 while TiO_2 and CaO present negative correlation with SiO_2 (Fig. 9). Moreover, Cr and Ni show negative correlation with SiO_2 while Rb, Ba, and Y are showing positive correlation with SiO_2 (Fig. 9).

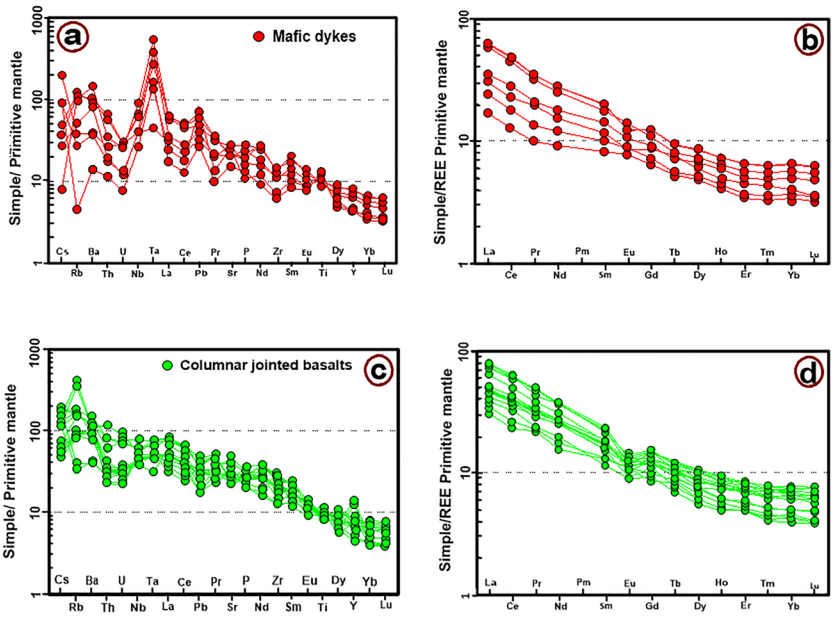

Fig. 10 Primitive mantle-normalized patterns for the studied mafic rocks [42]. **a** Trace element patterns of the columnar jointed basalts, **b** REE patterns of the columnar jointed basalts, **c** Trace element patterns of the mafic dykes, **d** REE patterns of the mafic dykes

The mafic dykes show high Ni (86–240 ppm) and Cr (133 to 295 ppm) concentrations and low to moderate Co (29–52 ppm) contents. On the multi-element diagram normalized to primitive mantle abundances given by McDonough and Sun [42], the mafic dyke samples show positive anomalies in Rb, Ba, Nb, Ta, Ti and Pb, and negative anomalies in Th, U, Ce, and Zr (Fig. 10c). The REE diagram normalized to the primitive mantle [42] shows a slight fractionation, and is enriched in LREE ($La_N/Sm_N = 2.07–3.38$) compared to HREE ($Gd_N/Yb_N = 1.87–2.19$) (Fig. 10d). They also show negative to slight positive europium anomalies ($(Eu/Eu^*)_N = 0.76$ to 1.01).

5 Discussion

5.1 Alteration

After magma emplacement and crystallization, some alteration processes can take place in the rock. The effect of that alteration can be seen either in thin sections or in LOI values or trace elements ratios. Some indications of alteration are seen in few thin sections such as chloritisation of pyroxene and serpentinization of olivine. However, most samples remain largely unaltered. The LOI (1–7 wt%) of all the studied rocks indicates that the samples were subjected to variable degrees of alteration (Table 3). Moreover, the Y/Ho ratios can also be used for evaluating the role of alteration. The Y/Ho ratio is varying from 22 to 36 in the columnar jointed basalts (with three samples presenting the value > 44) and from 24 to 31 in mafic dykes. The mean value (Y/Ho = 31) of all the columnar jointed basalts and mafic dykes are slightly over the value of 28 that is observed in fresh basaltic rocks [43] and below the values observed in altered rocks (between 44 and 74) [44, 45] indicating globally that secondary processes were not significant on the studied rocks.

5.1.1 Crustal contamination

Understanding the nature of the mantle source and the petrogenetic processes requires a good understanding of the role of crustal contamination. In the wide range, the major oxides and LILE compositions generally change during the post-magmatic processes. The overall variations in concentrations of major oxides, LILE, HFSE and LREEs can be caused by crustal contamination [46].

Trace elements chemistry is a good proxy to assess crustal contamination. Mafic magma affected by crustal contamination generally presents Ti and P depletion and enrichment of Th and LREEs (e.g., [47]). The studied mafic dykes and columnar do not have large P and Ti troughs on primitive mantle-normalized multi-element diagrams (Fig. 10a, c), testifying

to insignificant or minor crustal input in the magma. The low concentrations of U and Th in the studied dykes may also point to a lack of significant crustal contamination [48]. The mafic dyke samples show low Ba contents (mean = 483 ppm) and low Lu/Yb (0.13 -0.14) ratio while the columnar jointed basalts display slightly high Ba (mean = 647) contents and Lu/Yb (0.13–0.16) ratio compared to the mid-continental crust [Ba = 259–628 ppm; and Lu/Yb (0.16–0.18)] [49]. These values may suggest possible small degree of crustal contamination on the columnar jointed basalts or the enrichment of those elements in the source. This low degree of contamination is also supported by the rapid crystallization of the columnar jointed basalts magma during quenching (highlighted by the high FeO content (18.24- 30.07 wt%) and low Al_2O_3 (0.13–0.58 wt%) and MgO (0.03–0.31 wt%) contents testifying to the substitution of Al^{3+} and Mg^{2+} by the Fe^{3+}) [30]. On the thin section, the low degree of contamination is evidenced by the presence of only a few occurrences of quartz xenoliths (probably taken from the crustal substratum) reacting with microcrysts of pyroxenes (Fig. 4b).

5.2 Magma processes

Some authors [50, 51] have demonstrated that high field strength elements (HFSE) such as Zr, Hf, Nb, Ta, Th, Y, P and Ti are stable even when they have undergone high-grade metamorphism. Large ion lithophile elements (LILE) such as Ba, Cs and Rb, on the other hand, have a strong crustal-mantle fractionation and may be unstable during metamorphism or crustal contamination during magma ascension, thus altering the physicochemical composition of the magma [52, 53]. Due to their relative stability during crustal contamination or metamorphism, transition metals and HFSEs are mainly used to study the tectonic settings and magma sources of rocks [54, 55]. The major element geochemistry of the studied mafic rocks demonstrates the calc-alkaline nature of the columnar jointed basalts and the mafic dykes (Fig. 8b). Plotted on the Ti versus (Ca + Na) diagram of pyroxenes after Leterrier et al. [56], the studied pyroxenes plot on the boundary between tholeiitic and alkali basalt fields, but mostly in the alkali basalt field (Fig. 11a). The columnar jointed basalts are basic to intermediate (SiO_2 = 46–52 wt%), and display low to moderate Mg# (40–53), Ni(35–173 ppm), Co (29–53 ppm) and Cr (87–268 ppm) while the mafic dykes are essentially basic (SiO_2 = 46–50 wt%), and display moderate to high Mg# (50–65), Ni (86–240 ppm), Co (29–52 ppm and Cr (133–295 ppm) (Table 3). These chemical compositions are lower than those of the average composition of primary mantle (Ni = 300–400 ppm, Co = 50–70 ppm, Cr = 300–500 ppm) [57]. These

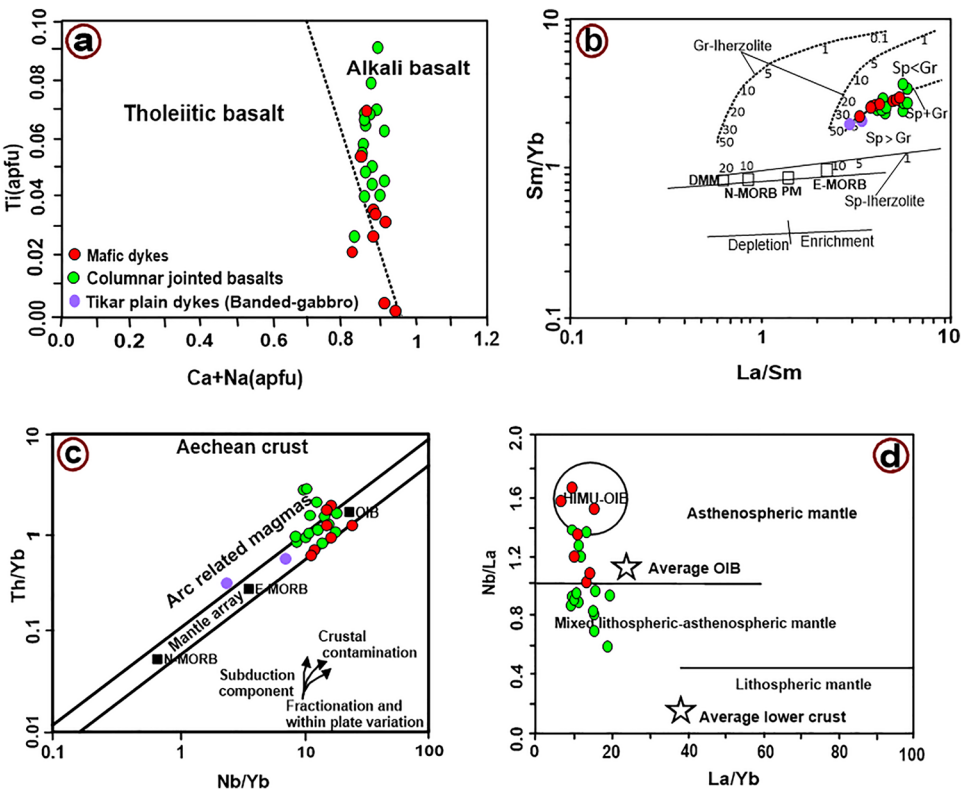

Fig. 11 **a** Ti versus (Ca + Na) diagram of pyroxenes after Leterrier et al. [56], **b** La/Sm versus Sm/Yb diagram for the studied dykes. Melting curves for garnet and spinel lherzolite are after Aldanmaz et al. [61]. Numbers along the curves represent the percentage of partial melting for different proportions of garnet (Gt) and spinel (Sp), **c** Th/Yb versus Nb/Yb diagram [62], **d** Nb/La versus La/Yb variation diagram for the studied mafic rocks

major elements and trace element characteristics indicate that the studied rocks had undergone fractionation, with the mafic dykes being the least fractionated.

Moreover, on the plot of SiO_2 (wt%) versus other major and trace elements, Al_2O_3, K_2O, Y and Ba show a positive correlation with SiO_2, while MgO, CaO, TiO_2, Ni and Cr display a negative correlation with SiO_2, demonstrating the crystallization process especially the fractionation of olivine and clinopyroxene [57] (Fig. 9). The studied mafic rocks present negative to slightly positive Eu anomalies (Eu/Eu* = 06–1.03) indicating plagioclase fractionation.

5.3 Partial melting and magma source

Culler [58] has shown that the profiles of the REE patterns are important to better understand the melting conditions of the rock. Thus, a low melting percentage of the magma source can produce slightly tilted REE patterns, while a higher degree of mantle melting produces flat REE patterns [59]. Furthermore, the inclined profile of REE can also indicate the origin of an enriched mantle source, whereas the flat profiles may demonstrate a depleted mantle source. The REE profiles of the columnar jointed basalts and mafic dykes exhibit a relatively tilted pattern, suggesting a low degree of partial melting of an enriched mantle source. The REE pattern of the mafic dykes and columnar jointed basalts are quite similar and may indicate the same source for their magmas. This assumption is also strongly supported by the relatively high Dy/Yb ratios (~ 2, mean = 2.14 for the mafic dykes and mean = 2.09 for the columnar jointed basalts) of the studied rocks, implying that partial melting could have taken place in the spinel-garnet transition zone [60]. This hypothesis is also supported by the (La/Sm) versus (Sm/Yb) diagram after Aldanmaz et al. [61], which shows the columnar jointed basalts and the mafic dyke samples falling near the E-MORB domain following the spinel + garnet line (Fig. 11b). The studied samples also plot mostly along the mantle array of the Nb/Yb versus Th/Yb diagram [62], with few columnar jointed basalts samples extending on the arc related magma area, consolidating the mantle source for the studied mafic rocks (Fig. 11c). Moreover, the Ce/Pb ratios of the studied samples vary from 7 to 23 for the columnar jointed basalts and from 5 to 10 for the mafic dykes (except one sample with Ce/Pb value of 2.78). These values are lower than the average values obtained from the basaltic lavas from the Cameroon Volcanic Line (25–32) and also lower than MORB and OIB values (25 ± 5, [63], but they are higher than the average value found in the upper-crust (3.2, [64]). The trace element compositions of the columnar jointed basalts and mafic dykes show some visible differences. The columnar jointed basalts show a relative depletion in Nb, Ta and Pb on the primitive mantle normalized multi-element plot (Fig. 10a) while the mafic dykes display pronounced enrichment in Nb, Ta and Pb (Fig. 10c). These features suggest a certain degree of evolution or contamination of the columnar jointed basalts compared to the mafic dyke samples.

Considering the characteristics of the trace elements composition of the columnar jointed basalts, the following deduction could be made, firstly of (1) a mixture of a plume-like melt with the continental crust or; (2) plume-like melt with the sub-continental lithospheric mantle to produce the columnar jointed basalts. However, when the mixing involves the continental crust, very significant Nb–Ta negative anomalies appear on the PM-normalized multi-element patterns for the studied rocks, which is not the case here.

Moreover, the plume-derived melts generally have a low La/Ta ratio (8–15). When this value is much higher (> 25 in general), it indicates the involvement of the Sub-continental lithospheric mantle (SCLM). Also, the melts contaminated by crustal materials generally exhibit high La/Sm ratio (> 5) [65]. The studied mafic dykes display low La/Ta ratios (mostly < 12) and low La/Sm ratios (< 5) testifying to its plume source while the columnar jointed basalts present varying La/Ta ratios (10 to 20 with one sample with the value of 37) and low La/Sm ratio (3 to 5) suggesting the participation of the SCLM to their formation.

Furthermore, the studied samples from the Mfengou-Manki area are depleted in incompatible element and have the La/Nb ratios (0.6–1.7), Th/Nb (0.04–0.25), Zr/Nb (2.56–9.27) and Ba/Nb (5.31–25.86). These ratios are lower than those of the continental crust and very close to those of the OIB, indicating the OIB-type geochemical signatures for the studied mafic rocks [66].

The columnar jointed basalts display low Nb/La (< 1) ratio while the mafic dykes display high Nb/La (> 1) ratio suggesting the participation of the lithospheric mantle source to the genesis of the columnar jointed basalts and exclusively the OIB-like asthenospheric mantle for the mafic dykes [67, 68]. This result is also supported by the Nb/La versus La/Yb diagram (Fig. 11d), in which the mafic dykes plot mainly on the HIMU-OIB asthenospheric mantle and the columnar jointed basalts samples plotting mainly on the mixed lithospheric-asthenospheric mantle area.

Also, studied mafic rocks display moderate TiO_2 contents (between 1.69 and 2.29 wt.% for the columnar jointed basalts and 1.87–2.64 wt.% for the mafic dykes) and characterize magmas generated from a slightly shallower mantle source

compared to high-Ti magmas. It has been demonstrated that high-Ti content in basalts are evidence for the involvement of asthenospheric mantle source components in the genesis of the basaltic rocks [69, 70]. It is therefore very likely that the studied columnar jointed basalts were generated by shallow melting of asthenospheric mantle source mixed with different amounts of melts from SCLM.

The geochemical composition of the plume-derived melts may have been imparted into SCLM through the plume-lithosphere interaction especially during the delamination process [70, 71]. So, the contamination of asthenospheric magma by lithosphere-derived melt probably played an important role in the genesis of the studied columnar jointed basalts as demonstrated on the Soltan Maidan basalts in Iran [72].

This geological phenomenon is not new in Cameroon. The mixing of source material from the asthenospheric and the lithospheric mantle has also been previously mentioned in some areas of the Cameroon Volcanic Line such as the Bioko island [73], the Mts Bambouto and Oku, the Ngaoundere Plateau [74], and the Bamenda Mountains [75].

5.4 Comparison with the other mafic dykes in the Cameroon Central Shear Zone

The geochemical and mineralogical characteristics of the Mfengou-Manki columnar jointed basalts and mafic dykes compared to those of other dykes in the Central African Fold Belt in Cameroon reveal some differences and similarities. The studied mafic rocks present silica content (46% to 52%) similar to those from the Njimom area (46–51%), but high Ni (86–240 ppm) and Cr (133–295 ppm) content compared to those of Njimom dykes (Ni = 30–110 ppm; Cr = 70–180 ppm) [19].

The mafic dykes from the Tikar Plain and Kekem areas derived from the sub-continental lithospheric mantle source [26, 76] and are indeed different from the Mfengou-Manki mafic dykes and columnar jointed basalts that originated from asthenospheric and mixed asthenospheric-lithospheric mantle respectively. The studied mafic dykes, compared to the columnar jointed basalts, are more enriched in Nb, Ta Ti and Sr, but depleted in Zr compared to the Tikar plain and Kekem dykes, (Fig. 12a, b).

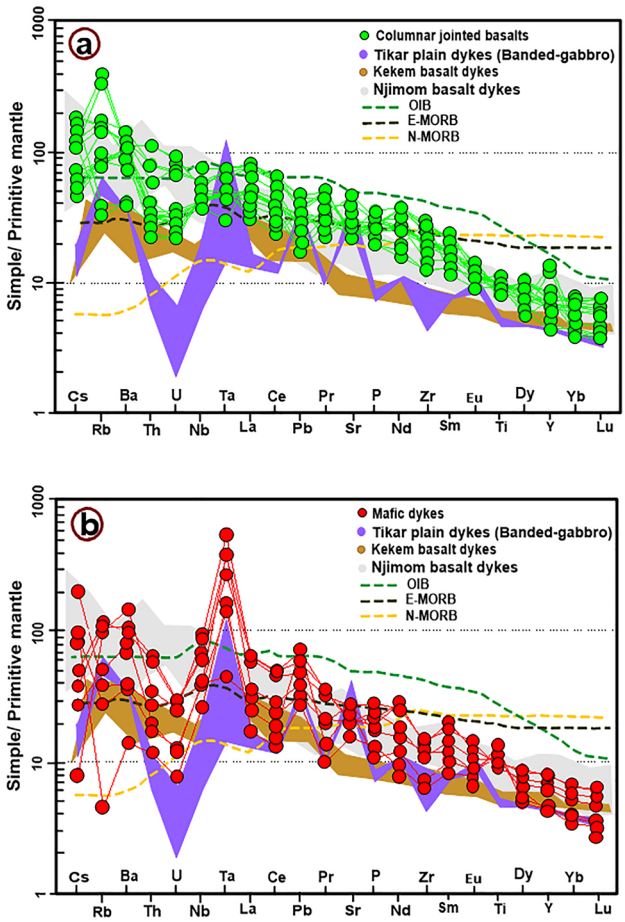

Fig. 12 **a** Primitive mantle-normalized trace elements for the Mfengou-Manki columnar jointed basalts compared to the Tikar plain, Kekem and Njimom dykes, **b** Primitive mantle-normalized trace elements for the Mfengou-Manki mafic dykes compared to the Tikar plain, Kekem and Njimom dykes

From the field relationship, the mafic dykes are oriented parallel to the Tikar plain dykes and Kekem dykes (NW–SE direction) and are perpendicular to the direction of the Cameroon Volcanic Line (NE-SW). That direction is similar to that of the second deformation phase (D_2) in the CCSZ dominated by the shearing movement [26]. The C_2 shear axes (NW–SE) of the second deformation phase in the Central Cameroon Shear Zone may have favored the emplacement of the studied dykes as it is the case for the Tikar plain mafic dykes.

5.5 Tectonic setting and geodynamic implication in the Cameroon Volcanic Line and Central Cameroon Shear Zone

The geochemistry of a specific type of magmatic rock may reflect or indicate its tectonic setting [77]. Trace elements such as Nb, Y, Ta, Th, Sm, Zr, Hf, and Yb are generally used for the discrimination of the tectonic environment in which the rock has been formed. This is because of their relative stability and low ion energy potential during metamorphism and weathering processes. Using some of those elements (Nb, Zr, Y, Th, Hf), for the tectonic discrimination triangular diagrams (Hf/3-Th-Nb/16) after Wood [78] (Fig. 13), the studied samples fall within the E-MORB and within-plate tectonic domains. According to Rudnick and Gao [79], negative Ti, Ta and Nb anomalies are typical of continental crust and rocks whose chemical composition has been modified by subduction [80]. The enrichment in Nb, Ti and Ta of the mafic dykes exclude a contribution of the subducted slab to their formation [81, 82]. In contrast, the columnar jointed basalts show relatively negative anomalies in Nb and Ta, testifying to the little participation of the sub-continental lithospheric mantle in their formation.

The dykes may have intruded along lower to mid-crustal sub-vertical feeder channels and were emplaced along the shear axes during the C_2 shearing stage in the Adamawa Yade domain of the Central African Fold Belt in Cameroon [26]. This hypothesis is also supported by several authors indicating that the Pan African orogeny that affected the Neoproterozoic granitic basement of the Cameroon Line favored the emplacement of fractures and zones of weaknesses [24, 74, 83, 84] that have facilitated the emplacement of extrusive (lava flow and columnar) and intrusive magmatic (mafic dykes and anorogenic complexes) rocks [85]. Moreover, recent geophysical studies on the Central African Fold Belt in Cameroon demonstrated the existence of both the subduction, slab detachment and the delamination of the sub-continental lithospheric mantle under the Adamawa Yade domain and the West Cameroon domain ([86], Fig. 14).

6 Conclusion

The aim of this work was to study the petrography, geochemistry and mineral chemistry of the mafic dykes and the columnar jointed basalts, in order to constrain their petrogenesis and tectonic settings and the role of lithospheric or asthenospheric source in their genesis. Two hypotheses have been proposed for the origin of the columnar jointed

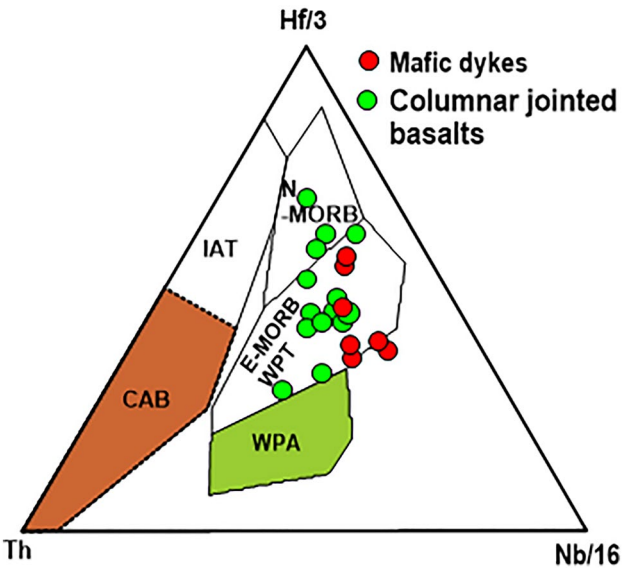

Fig. 13 Hf/3-Th-Nb/16 tectonic classification diagram of the studied mafic rocks [78]

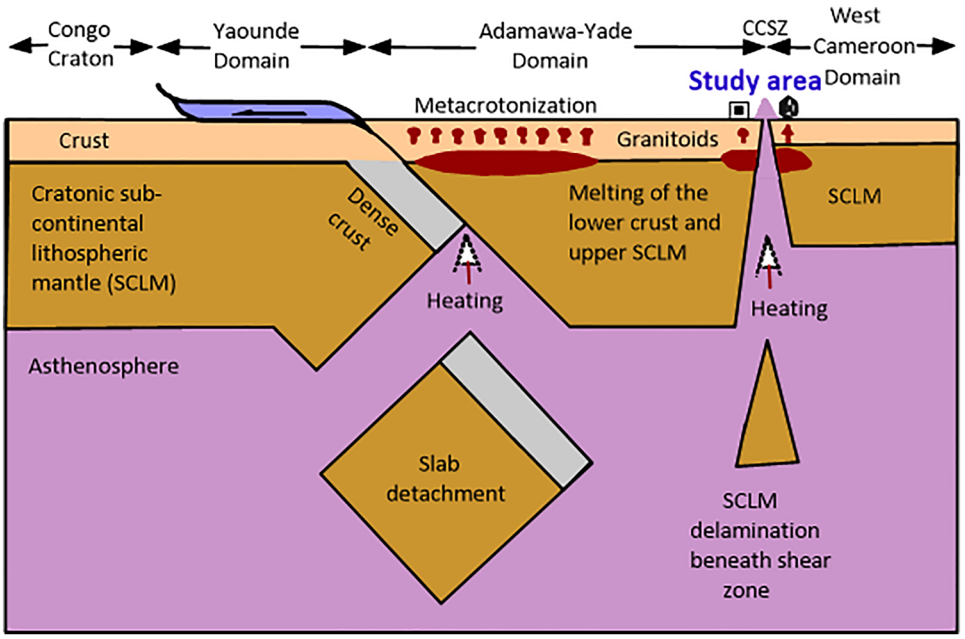

Fig. 14 Schematic model modified from Goussi Galamo et al. [87] showing the subduction involving the Congo Craton and the Adamawa-Yade domain and the delamination of the SCLM under the Central Cameroon Shear Zone. The SCLM delamination favoured the mixing between the plume and the SCLM magmas leading to the formation of columnar jointed basalts. The mafic dykes followed the fracture of the shear zone to be emplaced at the surface and sub-surface without significant contamination

basalts: (1) a mixture of a plume-like melt with the continental crust or (2) plume-like melt with the sub-continental lithospheric mantle.

The petrography and geochemistry of the Mfengou-Manki mafic rocks permitted to highlight two main mafic rock types, namely the mafic dykes and the columnar jointed basalts. The mafic dykes present fine to medium-grained texture while the columnar jointed basalts display the microlitic texture. The mafic dykes are calc-alkaline while the columnar jointed basalts are calc-alkaline to tholeiitic in nature. The geochemistry of the analyzed samples indicates that the mafic dykes are from the asthenospheric mantle source while the columnar jointed basalts are from the mixed lithospheric-asthenospheric mantle.

The mafic dykes emplaced at a temperature of 1071 to 1193 °C and a pressure of 4 to 12 kbar while the columnar jointed basalts emplaced at a temperature of 1064 to 1152 °C and 2 to 13 kbar pressure.

The studied rocks emplaced in the within-plate domain following the C_2 shear axes in the Cameroon Central Shear Zone. The delamination of the sub-continental lithospheric mantle under the Central Cameroon Shear Zone in the Adamawa Yade domain and the West Cameroon domain may have favored the ascend of the plume-derived melts which imparted into SCLM through the plume-lithosphere interaction. However, the petrography, whole-rock geochemistry and mineral chemistry alone are not sufficient to better explain the magma sources and processes leading to the formation of such complex geochemical features. Isotopic and geochronological studies should be done respectively in the future work to better constrain the magma sources, the mixing processes and the emplacement ages of the studied mafic rocks.

Acknowledgements This paper is a part of the first author's PhD thesis in preparation. We would like to thank anonymous reviewers for their constructive corrections. The authors thank Professor Jacques-Marie Bardintzeff for the EPMA analyses at Camparis, Université Pierre et Marie Curie, Paris.

Author contributions ZN: field work, manuscript writing and funding for analyses; BN: field work and manuscript review; RYF: manuscript review, MN: field work and geochemical analysis financement; MAM: fieldwork and thin section financement, CGSA work and graph work, MNAO: field work and graph work and MA: manuscript review.

Funding Funding for this work was provided by authors and EPMA analyses by Professor Jacques- Marie Bardintzeff.

Data availability The datasets generated during the current study are available from the second author (Dr NTIECHE Benjamin, E-mail; ntiechebenjo@yahoo.fr) on reasonable request.

Declarations

Competing interests The authors declare no competing of interest that may influence this work.

References

1. Wang BD, Wang LQ, Chung SL, Chen JL, Yin FG, Liu H, Li XB, Chen LK. Evolution of the Bangong-Nujiang Tethyan Ocean: insights from the geochronology and geochemistry of mafic-intermediate rocks within ophiolites. Lithos. 2016;245:18–33. https://doi.org/10.1016/j.lithos.2015.07.016.
2. Kamei A, Owada M, Nagao T, Shiraki K. High-mg diorites derived from sanukitic HMA magmas, Kyushu Island, Southwest Japan arc: evidence from clinopyroxene and whole rock compositions. Lithos. 2004;75:359–71. https://doi.org/10.1016/j.lithos.2004.03.006.
3. Karsli O, Dokuz A, Uysal I, Aydin F, Chen B, Kandemir R, Wijbrans J. Relative contributions of crust and mantle to generation of Campanian high-K calc-alkaline I type granitoids in a subduction setting, with special reference to the Harsit pluton, eastern Turkey. Contrib Mineral Petrol. 2010;160:467–87. https://doi.org/10.1007/s00410-010-0489-z.
4. Chung SL, Bm J. Plume–lithosphere interaction in generation of the Emeishan flood basalts at the Permian-Triassic boundary. Geology. 1995;23:889–92. https://doi.org/10.1130/0091-7613(1995)023%3c0889:PLIIGO%3e2.3.CO;2.
5. Song X, Hou Z, Zhimin C, Lu J, Wang Y, Zhang C, Li Y. Geochemical characteristics and period of the Emei Igneous province. Acta Geol Sin. 2001;75:498–506.
6. Xu Y, Chung SL, Jahn Bm WuG. Petrologic and geochemical constraints on the petrogenesis of Permian-Triassic Emeishan flood basalts in Southwestern China. Lithos. 2001;58:145–68. https://doi.org/10.1016/S0024-4937(01)00055-X.
7. Zhang ZC, Wang FS. Geochemistry of two types of basalts of the Emeishan basaltic province: evidence for mantle plume–lithosphere interaction. Acta Geol Sin. 2002;76:138–47.
8. Saunders AD. Large igneous provinces: origin and environmental consequences. Elements. 2005;1:259–63. https://doi.org/10.2113/gselements.1.5.259.
9. Jourdan F, Bertrand H, Féraud G, Le Gall B, Watkeys M. Lithospheric mantle evolution monitored by overlapping large igneous provinces: case study in Southern Africa. Lithos. 2009;107:257–68. https://doi.org/10.1016/j.lithos.2008.10.011.
10. Whalen L, Gazel E, Vidito C, Puffer J, Bizimis M, Henika W, Caddick MJ. Super continental inheritance and its influence on super continental breakup: the Central Atlantic Magmatic Province and the breakup of Pangea. Geochem Geophys Geosyst. 2015;16:3532–54. https://doi.org/10.1002/2015GC005885.
11. Anderson DL. The sublithospheric mantle as the source of continental flood basalts; the case against the continental lithosphere and plume head reservoirs. Earth Planet Sci Lett. 1994;123:269–80. https://doi.org/10.1016/0012-821X(94)90273-9.
12. Falloon TJ, Danyushevsky LV, Crawford AJ, Maas R, Woodhead JD, Eggins SM, Bloomer SH, Wright DJ, Zlobin SK, Stacey AR. Multiple mantle plume components involved in the petrogenesis of subduction related lavas from the northern termination of the Tonga Arc and northern Lau Basin: evidence from the geochemistry of arc and back arc submarine volcanics. Geochem Geophys Geosyst. 2007. https://doi.org/10.1029/2007GC001619.
13. Andersen T. Correction of common lead in U-Pb analyses that do not report 204Pb. Chem Geol. 2002;192:59–79. https://doi.org/10.1016/S0009-2541(02)00195-X.
14. Martin H. Adakitic magmas: modern analogues of Archaean granitoids. Lithos. 1999;46:411–29. https://doi.org/10.1016/S0024-4937(98)00076-0.
15. Sajona FG, Maury RC, Pubellier M, Leterrier J, Bellon H, Cotton J. Magmatic source enrichment by slab-derived melts in a young post-collision setting, central Mindanao (Philippines). Lithos. 2000;5:173–206. https://doi.org/10.1016/S0024-4937(00)00019-0.
16. Chabou MC, Sebai A, Féraud G, Bertrand H. Datation 40 Ar/39 Ar de la province magmatique de l'Atlantique central dans le Sud-Ouest Algérien. CR Geosci. 2007;339:970–8. https://doi.org/10.1016/j.crte.2007.09.011.
17. Gao S, Rudnick RL, Yuan H, Liu X, Liu Y, Xu W, Ling W, Ayers J, Wang X, Wang Q. Recycling lower continental crust in the North China Craton. Nature. 2004;432:892–7. https://doi.org/10.1038/nature03162.
18. Ntieche B, Ram Mohan M, Amidou M, Pauline WN, Mounjouohou MA, Nchouwet Z, Mfepat D. Petrochemical constrains on the origin and tectonic setting of mafic to intermediate dykes from Tikar plain, Central Cameroon Shear Zone. SN Appl Sci. 2021;3:211. https://doi.org/10.1007/s42452-021-04265-5.
19. Keutchafo NAK, Simeni NAW, Nforba BK, Noucoucouk AA, Sonmo JD, Tchaptchet DT, Tchouankoue JP, Cucciniello C. Petrology of Mafic Dykes from the Njimom Area (West-Cameroon): a contribution to the characterization of Late Paleozoic and Mesozoic Magmatism in the Southern Continental Part of the Cameroon Volcanic Line. Geosciences. 2021;12:12. https://doi.org/10.3390/geosciences12010012.
20. Nzenti JP, Barbey P, Macaudiere J, Soba D. Origin and evolution of the Late Precambrian high-grade Yaounde gneiss (Cameroon). Precamb Res. 1988;38:91–109. https://doi.org/10.1016/0301-9268(88)90086-1.
21. Nkoumbou C, Yonta-Ngouné C, Villiéras F, Njopwouo D, Yvon J, Ekodeck GE, Tchoua F. Découverte de roches à affinité ophiolotique dans la chaîne panafricaine du Cameroun : les talcshistes de Ngoung, Lamal Pougué et Bibodi Lamal. CR Geosci. 2006;338:1167–75. https://doi.org/10.1016/j.crte.2006.07.008.
22. Toteu SF, Penaye J, Poudjom Djomani Y. Geodynamic evolution of the Pan-African belt in central Africa with special reference to Cameroon. Can J Earth Sci. 2004;41:73–85. https://doi.org/10.1139/e03-079.

23. Penaye J, Kröner A, Toteu SF, Van Schmus WR, Doumnang JC. Evolution of the Mayo Kebbi region as revealed by zircon dating: an early (ca. 740 Ma) Pan-African magmatic arc in Southwestern Chad. J Afr Earth Sc. 2006;44:530–42. https://doi.org/10.1016/j.jafrearsci.2005.11.018.
24. Toteu SF, Michard A, Bertrand JM, Dautel D. Metamorphic zircon from North-Cameroon: implication for the pan-African evolution of central Africa. Geol Rundsch. 1990;79(3):777–88. https://doi.org/10.1007/BF01879214.
25. Toteu SF, Yongué Fouateu R, Penaye J, Tchakounté J, Semé Mouangué AC, Van Schmus WR, Deloule E, Stendal H. U-Pb dating of plutonic rocks involved in the nappe tectonic in Southern Cameroon: consequence for the Pan-African fold belt. J Afr Earth Sc. 2006;44:479–93. https://doi.org/10.1016/j.jafrearsci.2005.11.015.
26. Ntiéche B, Moham MR, Moundi A. Granitoids of the Magba Shear Zone, West Cameroon, Central Africa: Evidences for Emplacement under Transpressive Tectonic regime. J Geol Soc India. 2017;89:33–46. https://doi.org/10.1007/s12594-017-0556-4.
27. Ntieche B, Wokwenmendam Nguet P, Moundi A, Ram Mohan M, Mounjouohou M, Atsalang CGS, Nchouwet Z. Arc magmatism in the Nkoula granitoid suites, Central African Fold belt in Cameroon: evidence of a metasomatized high oxidized S- and I- type magma. Int J Earth Sci. 2022. https://doi.org/10.1007/s00531-022-02175-4.
28. Njonfang E. Contribution à l'étude de la rélation entre la « Ligne du Cameroun » et la direction de l'Adamaoua: I- pétrologie et géochimie des formations magmatiques tertiaires associées. 2- pétrologie Géochimie et structure des granitoïdes panafricains de la zone de cisaillement Foumban-Bankim (Ouest Cameroun et Adamaoua). Thèse Doct d'Etat Univ. Yaoundé I. 1998. pp. 392.
29. Njonfang E, Ngako V, Kwekam M, Affaton P. Les orthogneiss calco-alcalins de Foumban-Bankim: témoins d'une zone interne de marge active panafricaine en cisaillement. Comptes Rendus Géosci. 2006;338:606–16. https://doi.org/10.1016/j.crte.2006.03.016.
30. Kuehner MS, Joswiak DJ. Naturally occuring ferric sanidine from the leucite Hills lamproite. Am Miner. 1996;81:229–37. https://doi.org/10.2138/am-1996-1-228.
31. Morimoto N, Fabrices J, Ferguson AK, Ginzburg IV, Ross M, Seifer FA, Zussman J, Akoi K, Gottard G. Nomenclature of pyroxenes". Min Mag. 1988;52:535–55. https://doi.org/10.1180/minmag.1988.052.367.15.
32. Soesoo AA. Multivariate statistical analysis of clinopyroxene composition: empirical coordinates for the crystallisation PT-estimations. Geol Soc Sweden (Geologiska Föreningen). 1997;119:55–60. https://doi.org/10.1080/11035899709546454.
33. Nimis P, Taylor WR. Single Clinopyroxene Thermobarometry for Garnet Peridotites. Part I. Calibration and testing of a Cr-in-Cpx barometer and an enstatite-in-Cpx thermometer. Contrib Min Petrol. 2000;139:541–54. https://doi.org/10.1007/s004100000156.
34. Helz RT. Phase relations of basalts in their melting ranges at PH2O= 5 kbar: part melt compositions. J Petrol. 1976;17:139–93. https://doi.org/10.1093/petrology/17.2.139.
35. Putirka K. thermometers and barometers for volcanic systems. Rev Mineral Geochem. 2008;69:61–120. https://doi.org/10.2138/rmg.2008.69.3.
36. Ngwa CN, Lenhardt N, le Roux P, Mbassa BJ. the Mount Cameroon southwest flank eruptions: geochemical constraints on the subsurface magma plumbing system. J Volcanol Geoth Res. 2019;384:179–88. https://doi.org/10.1016/j.jvolgeores.2019.07.016.
37. Kroll H, Evangelakakis C, Voll G. Two-feldspar geothermometery: a review and revision for slowly cooled rocks. Contrib Miner Petrol. 1993;114:510–8. https://doi.org/10.1007/BF00321755.
38. France L, Ildefonse B, Koepke J, Bech F. A new method to estimate the oxidation state of basaltic series from microprobe analyses. J Volcanol Geotherm Res. 2010;189:340–6. https://doi.org/10.1016/j.jvolgeores.2009.11.023.
39. Schweitzer EL, Papike JJ, Bence AE. Statistical analysis of clinopyroxenes from deep sea basalts. Am Mineral. 1979;64:501–13. https://doi.org/10.1029/GL005i007p00573.
40. Le Bas MJ, Le Maitre RW, Streckeisen A, Zanettin B. A chemical classification of volcanic rocks based on the total alkali-silica diagram. J Petrol. 1986;27(3):745–50. https://doi.org/10.1093/petrology/27.3.745.
41. Irvine TN, Baragar WRA. A guide to the chemical classification of the common volcanic rocks. Can J Earth Sci. 1971;8:523–48. https://doi.org/10.1139/e71-055.
42. Mc Donough WF, Sun SS. The composition of the earth. Chem Geol. 1995;120:223–53. https://doi.org/10.1016/0009-2541(94)00140-4.
43. Bau M. Controls on the fractionation of isovalent trace elements in magmatic and aqueous systems: evidence from Y/ho, Zr/Hf, and lanthanide tetrad effect. Contrib Min Pet. 1996;123:323–33. https://doi.org/10.1007/s004100050159.
44. Zhang J, Amakawa H, Nozaki Y. The comparative behaviors of yttrium and lanthanides in the seawater of the North Pacific. Geophys Res Lett. 1994;21:2677–80. https://doi.org/10.1029/94GL02404.
45. Bau M, Dulski P, Moller P. Yttrium and holmium in South Pacific seawater: vertical distribution and possible fractionation mechanisms. Chem Erde. 1995;55:1–15.
46. Wilson M. Igneous petrogenesis: a global tectonic approach. London: Chapman and Hall; 1993. p. 466. https://doi.org/10.1007/978-1-4020-6788-4.
47. Taylor SR, McLennan SM. The geochemical evolution of the continental crust. Rev Geophys. 1995;33:241–65. https://doi.org/10.1029/95RG00262.
48. Plank T. Constraints from thorium/lanthanum on sediment recycling at subduction zones and the evolution of the continents. J Petrol. 2005;46:921–44. https://doi.org/10.1093/petrology/egi005.
49. Gao JF, Lu JJ, Lai MY, Lin YP, Pu W. Analysis of trace elements in rock samples using HR-ICPMS. J Nanjing Univ (Nat Sci). 2003;39:844–50 (**in Chinese with English abstract**).
50. Pearce JA. Basalt geochemistry used to investigate past tectonic environments on Cyprus. Tectonophysics. 1975;25:41–67. https://doi.org/10.1016/0040-1951(75)90010-4.
51. Santosh M, Hu CN, He XF, Li SS, Tsunogae T, Shaji E, Indu G. Neoproterozoic arc magmatism in the southern Madurai block, India: subduction, relamination, continental outbuilding, and the growth of Gondwana. Gondwana Resvol. 2017;45:1–42. https://doi.org/10.1016/j.gr.2016.12.009.
52. Sun SS, McDonough WF. Chemical and isotopic systematics of oceanic basalts: implications for mantle composition and processes. In: Saunders AD, Norry MJ, editors. Magmatism in the Ocean Basins, vol. 42. London: Geological Society of Special Publication; 1989. https://doi.org/10.1144/GSL.SP.1989.042.01.19.

53. Staudigel H, Plank T, White B, Schmincke HU. Geochemical fuxes during sea floor alteration of the basaltic upper oceanic crust: DSDP sites 417 and 418. In: Bebout GE, Scholl SW, Kirby SH, Platt JP, editors. Subduction top to bottom. Washington DC: American Geophysical Union; 1996. p. 19–38.
54. Pearce JA, Cann JR. Tectonic setting of basic volcanic rocks determined using trace element analyses. Earth Planet Sci Lett. 1973;19:290–300. https://doi.org/10.1016/0012-821X(73)90129-5.
55. Jochum KP, Verma SP. Extreme enrichment of Sb, Tl, and other trace elements in altered MORB. Chem Geol. 1996;130:289–99. https://doi.org/10.1016/0009-2541(96)00014-9.
56. Leterrier J, Maurry RC, Thonon P, Girard D, Marchal M. Clinopyroxene composition as a method of identification of the magmatic affinites of paleo- volcanic series. Earth Planet Sci Lett. 1982;59:139–54. https://doi.org/10.1016/0012-821X(82)90122-4.
57. Frey F, Green D, Roy S. Integrated models of basalt petrogenesis: a study of quartz tholeiites to olivine melilitites from South-Eastern Australia utilising geochemical and experimental petrological data. J Petrol. 1978;19:463–513. https://doi.org/10.1093/petrology/19.3.463.
58. Cullers RL, Graf JL. Rare earth elements in igneous rocks of the continental crust: predominantly basic and ultrabasic rocks. In: Henderson P, editor. Rare earth element geochemistry. Amsterdam: Elsevier; 1984. p. 237–74. https://doi.org/10.1016/B978-0-444-42148-7.50013-7.
59. Hirschmann MM, Ghiorso MS, Wasylenki LE, Asimow PD, Stolper EM. Calculation of peridotite partial melting from thermodynamic models of minerals and melts. Method and composition to experiments. J Petrol. 1998;39:1091–115. https://doi.org/10.1093/petroj/40.5.831.
60. Duggen S, Hoernle K, Van P, Bogaard D, Garbe AD. Post–collisional transition from subduction–to intraplate–type magmatism in the westernmost Mediterranean: evidence for continental–edge delamination of subcontinental lithosphere. J Petrol. 2005;46(12):1155–201. https://doi.org/10.1093/petrology/egi013.
61. Aldanmaz E, Pearce JA, Thirlwall MF, Mitchell JG. Petrogenetic evolution of late Cenozoic, post-collision volcanism in western Anatolia. Turkey J Volcanol Geotherm Res. 2000;102(1–2):67–95. https://doi.org/10.1016/S0377-0273(00)00182-7.
62. Pearce JA. Geochemical fingerprinting of oceanic basalts with applications to ophiolite classification and the search for Archean oceanic crust. Lithos. 2008;100:14–48. https://doi.org/10.1016/j.lithos.2007.06.016.
63. Hofmann AW, Jochum KP, Seufert M, White WM. Nb and Pb in oceanic basalts; new constraints on mantle evolution. Earth Planet Sci Lett. 1986;79:33–45. https://doi.org/10.1016/0012-821X(86)90038-5.
64. Taylor SR, McLennan SM. The continental crust: its composition and evolution. Oxford: Blackwell; 1985. p. 312. https://doi.org/10.1002/gj.3350210116.
65. Lassiter JC, DePaolo DJ. Plume/lithosphere interaction in the generation of continental and oceanic flood basalts: chemical and isotope constraints. In: Mahoney J, editor. Large igneous provinces: continental, oceanic, and planetary flood volcanism. Washington DC: American Geophysical Union; 1997. p. 335–55. https://doi.org/10.1029/GM100p0335.
66. Weaver BL. The origin of ocean island basalt end-member compositions: trace element and isotopic constraints. Earth Planet Sci Lett. 1991;104:381–97. https://doi.org/10.1016/0012-821X(91)90217-6.
67. Thompson RN, Morrison MA. Asthenospheric and lower lithospheric mantle contributions to continental extension magmatism: an example from the British Tertiary Province. Chem Geol. 1988;68:1–15. https://doi.org/10.1016/0009-2541(88)90082-4.
68. Smith EI, Sánchez A, Walker JD, Wang K. Geochemistry of mafic magmas in the Hurricane volcanic field, Utah: implications for small and large-scale chemical variability of the lithospheric mantle. Geol J. 1999;107:433–48. https://doi.org/10.1086/314355.
69. Barry TL, Saunders AD, Kempton PD, Windley BF, Pringle MS, Dorjnamjaa D, Saandar S. Petrogenesis of Cenozoic basalts from Mongolia: evidence for the role of asthenospheric versus metasomatised lithospheric mantle sources. J Petrol. 2003;44:55–91. https://doi.org/10.1093/petrology/44.1.55.
70. Song XY, Qi HW, Robinson PT, Zhou MF, Cao ZM, Chen LM. Melting of the subcontinental lithospheric mantle by the Emeishan mantle plume: evidence from the basal alkaline basalts in Dongchuan, Yunnan, Southwestern China. Lithos. 2008;100:93–111. https://doi.org/10.1016/j.lithos.2007.06.023.
71. He Q, Xiao L, Balta B, Gao R, Chen J. Variety and complexity of the Late-Permian Emeishan basalts: reappraisal of plume-lithosphere interaction process. Lithos. 2010;119:91–107. https://doi.org/10.1016/j.lithos.2010.07.020.
72. Derakhshi M, Habibollah G, Laicheng M. Geochemistry and petrogenesis of SoltanMaidan basalts (E Alborz, Iran): implications for asthenosphere-lithosphere interaction and rifting along the N margin of Gondwana. Chem Erde. 2017;77:131–45. https://doi.org/10.1016/j.chemer.2017.01.002.
73. Yamgouot FN, Déruelle B, Mbowou GIB, Ngounouno I, Demaiffe D. Geochemistry of the volcanic rocks from Bioko Island ("Cameroon Hot Line"): evidence for plume-lithosphere interaction. Geosci Front. 2016;7(5):743–57. https://doi.org/10.1016/j.gsf.2015.06.003.
74. Marzoli A, Piccirillo E, Renne P, Bellieni G, Iacumin M, Nyobe J, Tongwa A. The Cameroon volcanic line revisited: petrogenesis of continental basaltic magmas from lithospheric and asthenospheric mantle sources. J Petrol. 2000;41:87–109. https://doi.org/10.1093/petrology/41.1.87.
75. Kamgang P, Chazot G, Njonfang E, Ngongang NBT, Tchoua FM. Mantle sources and magma evolution beneath the Cameroon volcanic line: geochemistry of mafic rocks from the Bamenda Mountains (NW Cameroon). Gondwana Res. 2013;24:727–41. https://doi.org/10.1016/j.gr.2012.11.009.
76. Tchaptchet TD, Wambo Simeni NA, Keutchafo Kouamo NA, Tchouankoue JP, Cucciniello C. Geology, mineralogy and geochemistry of the Kekem dyke swarm (Western Cameroon): insights into Paleozoic-Mesozoic magmatism and geodynamic implications. Comp Rend Geosci. 2017;349:175–85. https://doi.org/10.1016/j.crte.2017.02.005.
77. Dong X (2008) Geochronology and geochemistry of the Mesozoic and Cenozoic granites in the southwestern part of the Gangdese belt, Tibet. Master dissertation, China University of Geosciences (Bei- jing) (**in Chinese and abstract in English**)
78. Wood DA. The application of a Th Hf Ta diagram to problems of tectonomagmatic classification and to establishing the nature of crustal contamination of basaltic lavas of the British Tertiary Volcanic Province. Earth Planet Sci Lett. 1980;50:11–30. https://doi.org/10.1016/0012-821X(80)90116-8.
79. Rudnick RL, Gao S. Composition of the continental crust. In: Rudnick RL, Holland HD, Turekian KK, editors. Treatise on geochemistry—the crust, vol. 3. Oxford: Elsevier; 2003.

80. Ernst RE, Bleeker W, Söderlund U, Kerr AC. Large igneous provinces and supercontinents: toward completing the plate tectonic revolution. Lithos. 2013;174:1–14. https://doi.org/10.1016/j.lithos.2013.02.017.
81. Zhao JH, Zhou MF. Geochemistry of Neoproterozoic mafic intrusions in the Panzhihua district (Sichuan Province, SW China): implications for subduction-related metasomatism in the upper mantle. Precambr Res. 2007;152:27–47. https://doi.org/10.1016/j.precamres.2006.09.002.
82. Cai K, Sun M, Yuan C, Zhao G, Xiao W, Long X, Wu F. Geochronological and geochemical study of mafc dykes from thenorthwest Chinese Altai: implications for petrogenesis and tectonic evolution. Gondwana Res. 2010;18:638–52. https://doi.org/10.1016/j.gr.2010.02.010.
83. Toteu SF, Van Schmus WR, Penaye J, Michard A. New U-Pb and Sm-Nd data from north-central Cameroon and its bearing on the pre-Pan African history of central Africa. Precambr Res. 2001;108:45–73. https://doi.org/10.1016/S03019268(00)00149-2.
84. Asaah ANE, Tetsuya Y, Hikaru I, Aka FT, Tamen J, Takeshi K, Tomohiro U, Takeshi H, Fozing EM. Geochemical composition of dykes along the Cameroon Line (CL): petrogenesis and similarities with the Central Atlantic Magmatic Province. Geochemistry. 2022. https://doi.org/10.1016/j.chemer.2022.125865.
85. Aka FT, Hasegawa T, Nche LA, Asaah ANE, Mimba ME, Teitchou I, Ngwa C, Miyabuchi Y, Kobayashi T, Kankeu B, Yokoyama T, Tanyileke G, Ohba T, Hell JV, Kusakabe M. Upper Triassic mafic dykes of Lake Nyos, Cameroon (West Africa) I: K-ar age evidence within the context of Cameroon line magmatism and the tectonic significance. J Afr Earth Sci. 2018;141:49–59. https://doi.org/10.1016/j.jafrearsci.2018.02.001.
86. Burke K. Origin of the Cameroon Line of volcano-capped swells. J Geol. 2001;109:349–62. https://doi.org/10.1086/319977.
87. Goussi Ngalamo JF, Bisso D, Abdelsalam MG, Atekwana EA, Katumwehe AB, Ekodeck GE. Geophysical imaging of metacratonizaton in the northern edge of the Congo craton in Cameroon. J Afr Earth Sc. 2017;129:94–107. https://doi.org/10.1016/j.jafrearsci.2016.12.010.
88. Smith JV, Brown WL. Feldspar minerals: second revised and extended. Berlin: Springer; 1988.